BIAXIAL COMPRESSIVE STRENGTH
OF ROCKS AS APPLIED TO STABILITY ANALYSIS
OF TUNNEL BOUNDARIES

NONGNUCHAMAS PANPHUANGKAEW

A Thesis Submitted in Partial Fulfillment of the Requirements for the

Degree of Master of Engineering in Civil, Transportation

and Geo-resources Engineering

Suranaree University of Technology

Academic Year 2022

กำลังกดในสองแกนของหินสำหรับประยุกต์ใช้
วิเคราะห์เสถียรภาพของผนังอุโมงค์

นางสาวนงนุชมาศ ปานพวงแก้ว

BIAXIAL COMPRESSIVE STRENGTH OF ROCKS AS APPLIED

TO STABILITY ANALYSIS OF TUNNEL BOUNDARIES

Suranaree University of Technology has approved this thesis submitted in partial fulfillment of the requirements for a Master's Degree.

Thesis Examining Committee

....

(Assoc. Prof. Dr. Pornkasem Jongpradist)

Chairperson

....
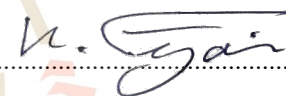
(Emeritus Prof. Dr. Kittitep Fuenkajorn)

Member (Thesis Advisor)

....

(Asst. Prof. Dr. Prachya Tepnarong)

Member

....

(Assoc. Prof. Dr. Chatchai Jothityangkoon)

Vice Rector for Academic Affairs and

Quality Assurance

....
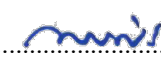
(Assoc. Prof. Dr. Pornsiri Jongkol)

Dean of Institute of Engineering

นงนุชมาศ ปานพวงแก้ว: กำลังกดในสองแกนของหินสำหรับประยุกต์ใช้วิเคราะห์เสถียรภาพ
ของผนังอุโมงค์ (BIAXIAL COMPRESSIVE STRENGTH OF ROCKS AS APPLIED TO
STABILITY ANALYSIS OF TUNNEL BOUNDARIES) อาจารย์ที่ปรึกษา: ศาสตราจารย์
(เกียรติคุณ) ดร.กิตติเทพ เฟื่องขจร, 84 หน้า.

คำสำคัญ: กำลังกดในสองแกน/ความเค้นหลักกลาง/กำลังรับแรง/ความยืดหยุ่น

การทดสอบในสองแกนและแกนเดียวได้ดำเนินการโดยใช้ตัวอย่างลูกบาศก์ของหินเก้าชนิด
โดยใช้โครงกดหินในสองแกน เพื่อหาผลกระทบของความเค้นหลักกลาง (σ_2) ต่อความแข็งของหิน ผล
การทดสอบบ่งชี้ว่าจากหินที่ทดสอบทั้งหมดนั้น σ_2 ส่งผลต่อความเค้นหลักที่จุดแตก กำลังกดของหิน
ที่สูงสุดอยู่ที่ค่าโหลด (L) ประมาณ -0.5, ที่ค่าต่ำกว่าและสูงกว่า L $= -0.5$ ความเค้นหลักที่จุดแตกมี
ค่าลดลง ตัวอย่างหินภายใต้ค่า σ_2 สูง แสดงการแตกแบบแยกภายใต้ความเค้นดึงในหลายแนวและ
ขนานกับระนาบของ $\sigma_1 - \sigma_2$ สามารถสังเกตได้ชัดเจนในหินที่แข็ง การรวมกันของการแตกแบบแยก
ของแรงดึงและแรงเฉือนสังเกตได้ภายใต้ค่า σ_2 ที่ต่ำ เกณฑ์การแตกของ Modified Wiebols and
Cook เพียงพอที่จะอธิบายกำลังกดในสองแกนภายใต้ค่าโหลดทั้งหมด ค่าความยืดหยุ่นและ
อัตราส่วนปัวซองไม่ขึ้นกับความเค้นหลักกลาง ค่ากำลังกดในสองแกนเหมาะสมกว่าค่ากำลังกดในแกน
เดียวในการนำมาประยุกต์เพื่อประเมินเสถียรภาพของผนังอุโมงค์ใต้ดิน

สาขาวิชา เทคโนโลยีธรณี   ลายมือชื่อนักศึกษา นงนุชมาศ
ปีการศึกษา 2565   ลายมือชื่ออาจารย์ที่ปรึกษา

NONGNUCHAMAS PANPHUANGKAEW: BIAXIAL COMPRESSIVE STRENGTH OF ROCKS AS APPLIED TO STABILITY ANALYSIS OF TUNNEL BOUNDARIES THESIS ADVISOR: EMERITUS PROF. KITTITEP FUENKAJORN, Ph.D. 84 PP.

KEYWORDS: BIAXIAL TEST/INTERMEDIATE PRINCIPAL STRESS/ROCK STRENGTHS/ELASTICITY

Biaxial and uniaxial tests have been performed on cubic specimens of nine rock types, using a biaxial loading device. The objective is to determine the effect of intermediate principal stress (σ_2) on rock strength. Results indicate that for all tested rocks σ_2 affects the major principal stress at failure. The maximum strengths are reached at Lode parameter (L) of about -0.5, below and above L $= -0.5$, the major principal stress at failure decreases. Post-test specimens under high σ_2 show multiple extensile fractures parallel to σ_1–σ_2 plane, particularly for strong rocks. Combination of extensile and shear fractures are observed under low σ_2. The modified Wiebols and Cook criterion is adequate to describe the biaxial compressive strengths under all Lode parameters. For all rock types, the elastic moduli and Poisson's ratios tend to be independent of the intermediate principal stress. Biaxial strengths obtained from laboratory are more appropriate to describe rock strengths at underground opening boundaries as compared to uniaxial strength.

School of Geotechnology

Academic Year 2022

Student's Signature....นงนุชมาศ........

Advisor's Signature....k.....

ACKNOWLEDGMENTS

I would like to express my sincere thanks to Emeritus Prof. Dr. Kittitep Fuenkajorn, thesis advisor, who gave a critical review and constant encouragement throughout the course of this research. Further appreciation is extended to Assoc. Prof. Dr. Pornkasem Jongpradist, Asst. Prof. Dr. Prachya Tepnarong, and who are members of my examination committee for their valuable suggestions and comments on my research works as thesis committee members. Grateful thanks are given to all staffs of Geomechanics Research Unit, Institute of Engineering who supported I work.

Finally, I most gratefully acknowledge my parents and friends for all their supported throughout the period of this research.

Nongnuchamas Panphuangkaew

TABLE OF CONTENTS

Page

TABLE OF CONTENTS (Continued)

LIST OF TABLES

LIST OF FIGURES

TABLE OF FIGURES (Continued)

LIST OF SYMBOLS AND ABBREVIATIONS

A = Parameter related to ϕ and σ_c of modified Wiebols and Cook criterion

A′ = Parameter related to τ_{oct} and $\sigma_{m,2}$ of Mogi criterion

B = Parameter related to ϕ and σ_c of modified Wiebols and Cook criterion

B′ = Parameter related to τ_{oct} and $\sigma_{m,2}$ of Mogi criterion

C = Cohesion related to ϕ and σ_c of modified Wiebols and Cook criterion

E = Elasticity or Elastic Modulus

f_1 = Function related to $\sigma_{m,2}$

FS = Factor of safety

G = Shear modulus

J_1 = First-order invariant of stress at failure

J_2 = Second-order invariant of stress at failure

L = Lode parameter

m = Number of data sets for calculated mean misfit

m = Parameter depended on rock materials of Hoek and Brown criterion

n = Number of intermediate principal stress or data points
for calculated mean misfit

P_0 = Uniform external stress

q = Parameter related to μ or ϕ of modified Wiebols and Cook criterion

s = Parameter depended on rock materials of Hoek and Brown criterion

LIST OF SYMOLS AND ABBREVIATIONS (Continued)

$\bar{s}$	=	Mean misfit
ε_1	=	Axial strain of σ_1
ε_2	=	Lateral strains of σ_2
ε_3	=	Lateral strains of σ_3
ε_v	=	Volumetric strain
ϕ	=	Internal friction angle
λ	=	Lame's constant
μ	=	Coefficient of internal friction (ϕ)
ν	=	Poisson's ratio
σ_1, $\sigma_{1,f}$	=	Maximum principal stress or major principal stress or failure stress
$\sigma_{1,j}^{calc}$	=	Maximum stress predicted from strength criterion
$\sigma_{1,j}^{test}$	=	Maximum stress from measured strengths
σ_2	=	Intermediate principal stress
σ_3	=	Minor principal stress or minimum principal stress
σ_c	=	Uniaxial compressive strength
$\sigma_{m,2}$	=	Effective mean stress related to σ_1 and σ_3 of Hoek and Brown criterion
σ_r	=	Radial stress
$\sigma_{Wiebols}$	=	Rock strengths according to the modified Wiebols and Cook criterion
σ_z	=	Axial stress
σ_θ	=	Tangential stress
τ_{oct}	=	Octahedral shear stress

CHAPTER I

INTRODUCTION

1.1 Background

The strength and elastic properties of rock are needed for design and analyze the stability of various underground structures. After excavation, the in-situ stress around tunnel is altered. Determination of stability of underground opening boundary usually relies upon uniaxial compressive strength of host rock. A limitation of such approach is that the intermediate principal stress (σ_2) is not taken into account. The triaxial test uses constant confining pressure at any depth as a representative in-situ stress. After excavation, the stress in all directions will change, and the rock condition around the tunnel is similar to biaxial stress state, but there are some misconceptions that often lead to the application of uniaxial compressive test data to represent the in-situ rock behavior which is lower than the actual value. It has been found that compressive strengths obtained from uniaxial testing may not represent the actual in-situ rock strength. This conventional analysis sometimes gives a non-conservative result.

1.2 Research objectives

The objective of this study is to determine the effects of intermediate principal stress on rock strength by biaxial test method. The results are used to assess the predictive capability of strength criteria developed by Hoek and Brown (1980), Mogi (1967), and modified Wiebols and Cook (1968). Biaxial strength tests are performed on specimens with nominal dimensions of 54x54x54 mm^3 using a biaxial loading frame. A biaxial loading frame is used to apply intermediate (σ_2) and minimum principal stress (σ_3) equal to zero on the rock specimen while the maximum principal stress (σ_1) is increased until failure. The rock types tested are commonly found in underground tunnels in Thailand, including granite, limestone, marble, gypsum, sandstone, and siltstone. Five specimens have been prepared for each rock type.

The sandstone and gypsum specimens are prepared to have bedding planes normal to the major principal direction. The specimen density is determined according to ASTM D7263–09 (2018).

1.3   Scope and limitations

The scope and limitations of the study include as follows.

1) Laboratory tests are performed on rock specimens; Korat group (Phra Wihan sandstone, Phu Phan sandstone and Phu Kradung siltstone), Tak batholiths, Lopburi formation, Saraburi formation, and Nakhon Sawan formation in Thailand.

2) Up to 45 samples are tested, on cubical specimens with nominal dimensions of 54x54x54 mm^3 (in length, width and height)

3) Uniaxial and biaxial tests are performed under dry condition with a biaxial loading frame.

4) The biaxial test is started by increasing σ_1 at a rate of 0.1 MPa/s. While maintain $\sigma_3 = 0$, σ_2 is increased at rates of 0.025, 0.05, 0.075 and 0.1 MPa/s for the Lode parameters (1926) of 0.5, 0, -0.5 and -1, respectively. The uniaxial compressive strength is obtained while maintaining $\sigma_2=\sigma_3=0$

5) Research findings had been published in conference paper or journal.

1.4   Research methodology

The research methodology comprises 6 steps (Figure 1.1); including literature review, sample preparation, uniaxial and biaxial compression test, development of strength criteria, discussions and conclusions, and thesis writing.

```
┌─────────────────────┐
│  Literature review  │
└─────────────────────┘
          │
          ▼
┌─────────────────────┐
│  Sample preparation │
└─────────────────────┘
          │
          ▼
┌──────────────────────────────────┐
│ Uniaxial and Biaxial compression test │
└──────────────────────────────────┘
          │
          ▼
┌──────────────────────────────────┐
│ Development of Strength Criterion │
└──────────────────────────────────┘
          │
          ▼
┌──────────────────────────────┐
│  Discussions & Conclusions   │
└──────────────────────────────┘
          │
          ▼
┌─────────────────────┐
│   Thesis writing    │
└─────────────────────┘
```
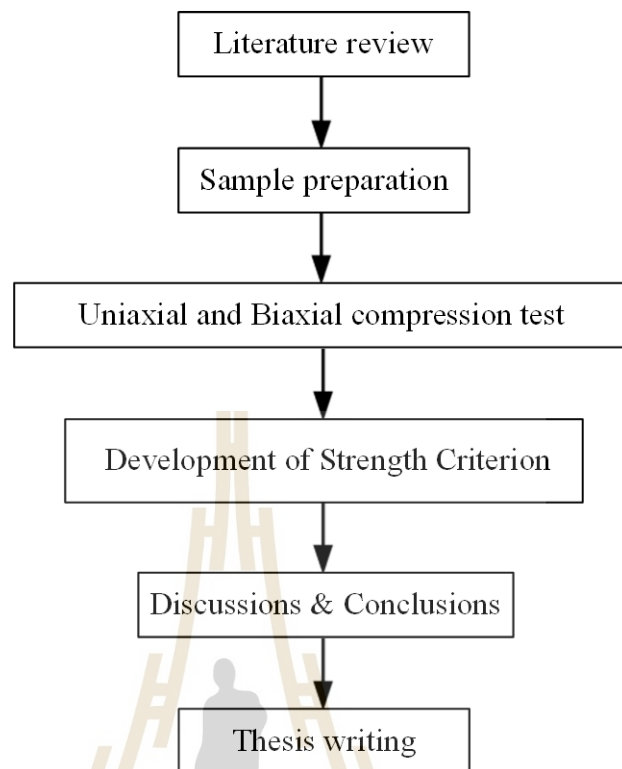
Figure 1.1 Test plan

1.4.1 Literature review

Literature review is carried out to study the previous researches on compressive strength in biaxial stress state and effect of intermediate principal stress (σ_2).

1.4.2 Sample preparation

Rock samples are commonly found in underground tunnels in Thailand, including Korat group (Phra Wihan sandstone, Phu Phan sandstone and Phu Kradung siltstone), Tak batholiths (granite), Lopburi formation (marble), Saraburi formation (limestone), and Nakhon Sawan formation (gypsum) in the northeastern Thailand. For sandstone and gypsum, bedding planes are normal to major direction. Cubic specimens are prepared with nominal dimensions of 54×54×54 mm^3. Five specimens have been prepared for each rock type.

1.4.3 Uniaxial and Biaxial testing

Biaxial loading frame (Fuenkajorn et al., 2012) has been used to apply axial stress (σ_1) and lateral stress (σ_2) on rock specimen shown in Figure 1.2. The frame comprises four main components; three mutually perpendicular steel load frames to secure rock specimens in the center, hydraulic cylinders, a measurement system and two hydraulic pumps. The measurement system is pressure gages and dial gages. The biaxial test is started by increasing σ_1 at a rate of 0.1 MPa/s. While maintain $\sigma_3 = 0$, σ_2 is increased at rates of 0.025, 0.05, 0.075 and 0.1 MPa/s for the Lode parameters of 0.5, 0, -0.5 and -1, respectively. The uniaxial compressive strength is obtained while maintaining $\sigma_2 = \sigma_3 = 0$. The tests are performed by increasing the axial stress until failure occurs. Neoprene sheets are placed at all interfaces between the loading platens and specimen surfaces to minimize friction.

1.4.4 Development of strength criteria

Results from laboratory testing in terms of the principal stresses at failure are used to formulate mathematical relations. The objective is to determine the strength parameters and elastic properties and to compare with three strength criteria include, modified Weibols and Cook (1968), Hoek and Brown (1980), and Mogi (1971) criteria. The predictive capability of the proposed strength criteria for the nine tested rocks is determined using the mean misfit ($\bar{s}$) as an indicator. The lower mean misfit value indicates good predictability.

1.4.5 Discussions and Conclusions

Comparison of results obtained from the testing of biaxial test with strength criterion. The proposed objective is discussed and evaluated.

1.4.6 Thesis writing

All research activities, methods, and results have been documented and incorporated in the dissertation.

Figure 1.2 True triaxial loading frame (Fuenkajorn et al., 2012)

1.5 Thesis contents

This research thesis is divided into seven chapters. The first chapter includes background and rationale, research objectives, scope limitations, and research methodology. Chapter II presents results of literature review to improve an understanding of rock compressive strength as affected by the intermediate principal stress. Chapter III describes sample preparation. Chapter IV describes test method of uniaxial and biaxial compressive strength test. Chapter V presents all test results. Chapter VI presents results from strength criteria calibration and compares with test results. Chapter VII is discussions, conclusions and recommendations for future studies.

CHAPTER II

LITERATURE REVIEW

2.1   Introduction

Relevant topics and previous research results are reviewed to improve an understanding the effects of intermediate principal stress (σ_2) on underground opening boundaries and the previous relevant testing. The contents are summarized below.

2.2   True triaxial compressive strength of rock

Wiebols and Cook (1968) study effect of intermediate principal stress (σ_2) on rock strength based on the earlier testing results. At first, there was an interest in the influence of σ_2 were made in 1960s by Murrell (1963) and Handin et al. (1967), which applied the results of triaxial compression-tension test. It was pointed out that σ_2 influences mechanical properties of rock because rock strength is larger in triaxial extension than in compression. Meanwhile, Handin et al. (1967) produced results similar to Murrell's indicating that rock strength was higher under larger intermediate principal stress ($\sigma_2 = \sigma_1$). As a result of previous experiments.

Alsayed (2002) conducts test on specimens of Springwell sandstone under different multiaxial stresses: including uniaxial, biaxial, triaxial, and polyaxial compression by using hollow cylinder (Figure 2.1). It can be used in many applications ranging from simulating stress conditions around underground openings to studying the behavior of rock under a much wider variety of stress paths. Under polyaxial and biaxial compressions, elasticity is adequate to describe the stress distribution in the test cylinders.
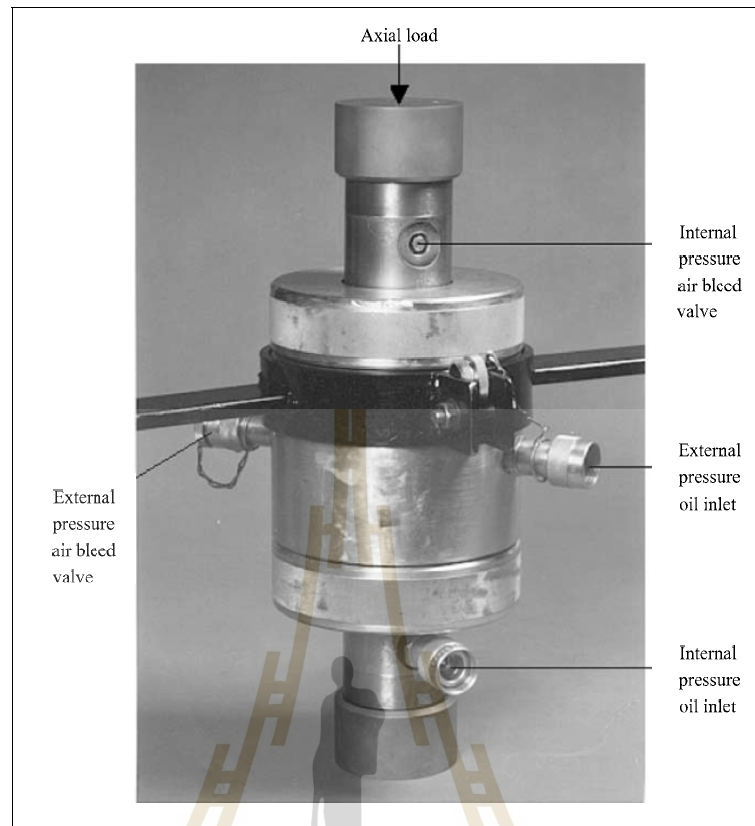
Figure 2.1 Test cell with a specimen inside (Alsayed, 2002)

Sahouryeh et al. (2002) use true triaxial cubicle cell (25x25x25 cm^3) and analyze results in three directions of crack propagation under biaxial compression at setting the load in one plane equal zero. Using sandstone, concrete and resin samples as rock samples. In biaxial stress cracking, the direction extends along the sample parallel to the free surface. This is consistent with all samples tested under this biaxial test, which states that σ_2 changes the mechanism of crack growth. The growth then becomes unstable, causing failure near the surface (Figure 2.2).

Figure 2.2 Splitting sample under biaxial compression (Sahouryeh et al., 2002)

Tiwari and Rao (2004) analyze the physical modeling of a rock mass under a true triaxial system (TTS) developed by Rao and Tiwari (2002) with the block model having three smooth joint sets. The results show that rock strength (σ_1) and deformation modulus increase, which is confirmed by fracture shear developed on σ_2. In addition, effect of interlocking and rotation of intermediate principal stress and minimum principal stress on strength and deformation response was also investigated.

Sriapai et al. (2011) determine true triaxial compressive strength of Maha Sarakham (MS) salt. The internal friction angle is determined from the triaxial loading ($\sigma_2 = \sigma_3$). The modified Lade criterion overestimates the actual strengths at all levels of σ_3. The results indicate modified Wiebols and Cook criterion can be best described effect of σ_2 on the salt strengths.

Khamrat et al. (2016) study the effect of pore pressure in dry and wet conditions with six rock types as shown in Table 2.1, with dimensions of 50x50x100 mm^3. The confining pressures range from 0 to 12 MPa under various loading rates 0.001-10 MPa. It shows that low loading rate causes compressive shear failure, but a higher loading rate would be an extension failure. Dry conditions give higher strength than wet ones due to the effect of pore pressure reducing compressive strength and elasticity while increases Poisson's ratio of rock.

Table 2.1 Rock properties by Khamrat et al. (2016)

Rock Unit	Rock Type	Location	σ_3 (MPa)	σ_1 (MPa)	C (MPa)	ϕ (°)	E (MPa)	ν
Phu Phan Formation (Red)	Sandstone	Nakhon Ratchasima, Thailand	0	80	17.6	43	11.1	0.29
			3	98				
			7	118				
			12	146				
Phu Phan Formation (Yellow)	Sandstone	Nakhon Ratchasima, Thailand	0	80	17.6	43	11.1	0.29
			3	98				
			7	118				
			12	146				
Phu Kradung Formation	Siltstone	Nakhon Ratchasima, Thailand	0	65	13.0	45	9.2	0.16
			3	83				
			7	105				
			12	134				
Phra Wihan Formation	Sandstone	Nakhon Ratchasima, Thailand	0	54	11.2	47	9.9	0.26
			3	73				
			7	103				
			12	130				
Tak Batholith	Granite	Tak, Thailand	0	70	9.4	60	10.1	0.32
			3	114				
			7	169				
			12	243				
Khao Khad Formation	Marble	Lopburi, Thailand	0	40	10.2	36	7.6	0.28
			3	53				
			7	69				
			12	88				

2.3 Biaxial compressive strength of rocks

Fakhimi et al. (2002) carry out testing on rectangular prism of sandstone with size 40x100x100 mm^3, with a center hole drilled with a diameter of 14 mm for a model an underground opening representing brittle rock by biaxial compression test (Figure 2.3). For simulation of failure on boundary an underground excavation in

brittle rock with numerical method by PFC2D (particle flow code). In addition to the measurement of failure, microcracking with AE (acoustic emission) method installed in the rock specimen. Cracking model and surface spalling can be easily simulated. The results of the simulated tunnel simulations are consistent with the test, corresponding to the values of the AE obtained that characterize fractures and show the orientation of the microcrack began to occur in the lateral walls of the tunnel and spread at an oblique angle to both sides where the microscopic cracks eventually formed to form shear cracks.
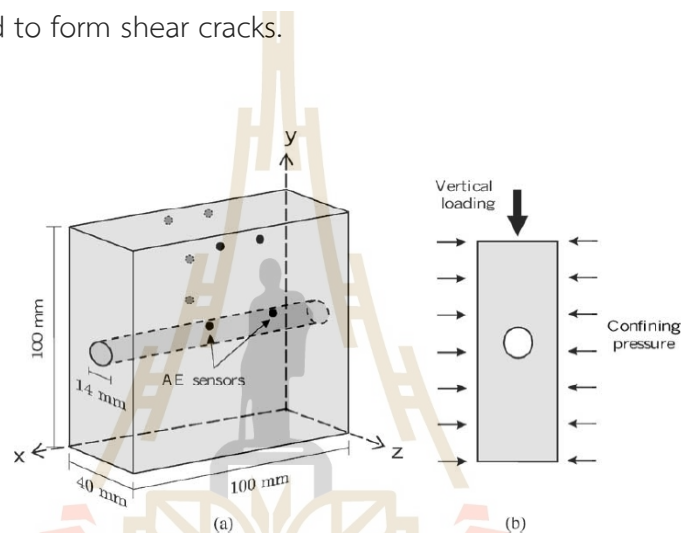
Figure 2.3   Model setup: (a) specimen and AE sensors; (b) loading direction (Fakhimi et al., 2002)

Zhu et al. (2005) study fracturing process of initiation around underground excavation under different loading conditions, using a numerical code called RFPA (rock failure process analysis), RFPA was used to simulate typical shapes of underground excavations, consisting of circular, elliptical and inverted U-shaped and simulate failure process of rocks in a number of engineering fields, in line with the well-researched Tang and Hudson (2002); Zhu and Tang, (2004). They explain that, for a circular opening under uniaxial compression (low lateral pressure) a primary tensile fracture and gradually shear crack, for elliptical opening, cracks are caused by tensile damage, as primary tensile cracks are extended and the U-shaped opening, the main tensile cracks are formed on the wall. The results model show that code can predict the patterns of fracture under various loading conditions.

Cai (2008) study the effects of σ_2 on rock fracture and rock strength near excavation boundaries by numerical method using a FEM/DEM. The simulation results indicate that the rock properties were homogeneous and that the tunnel was highly σ_2. Extremely high the σ_2 causes near excavation boundaries to cause microcrack. The numerical study is based on the stress test on rock samples that conform to the stress state, and also found that σ_2 has limitations influencing the maximum rock hardness in the tunnel surface.
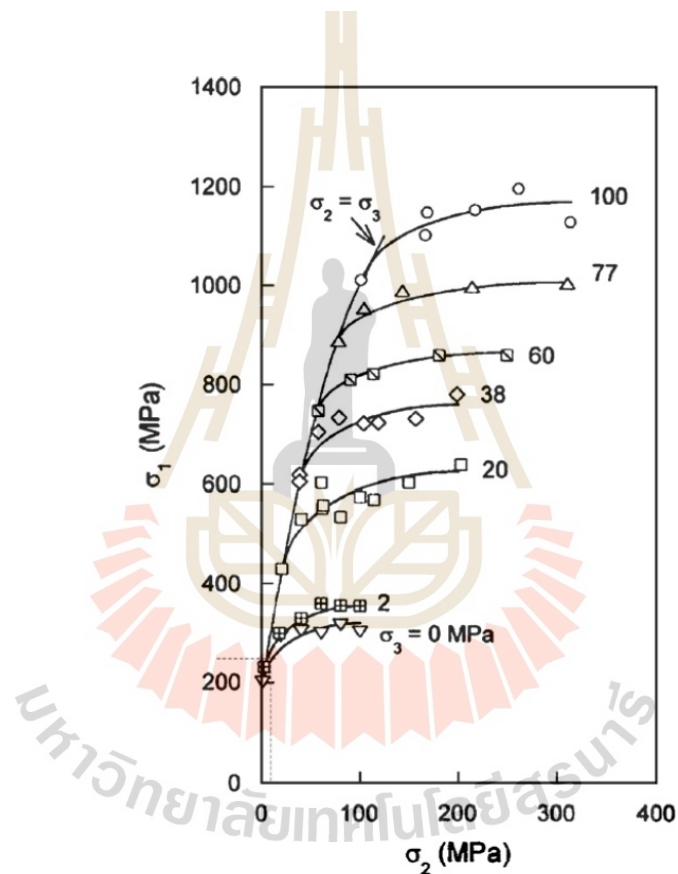
Figure 2.4 Effect of σ_2 on strength of Westerly granite (Cai, 2008)

Yun et al. (2010) test cubic intact granite with biaxial testing machine and comparison of the test results with Mohr-Coulomb and Hoek-Brown failure criteria showed these disregard the effect of σ_2. It is not reasonable for biaxial loading with the test results showed a poor correlation and agreed with Haimson and Rudnicki (2010), the increment of σ_2 is a form inconsistent with Mohr-Coulomb theory. And also, have been used Drucker–Prager criterion, which considers the effects of σ_2, this

is consistent with the study requested by Colmenares and Zoback (2002) was poorly correlated with biaxial test results and explained that the intensity and volume of the spalling plate increased with confinement pressure shown in Figure 2.5.
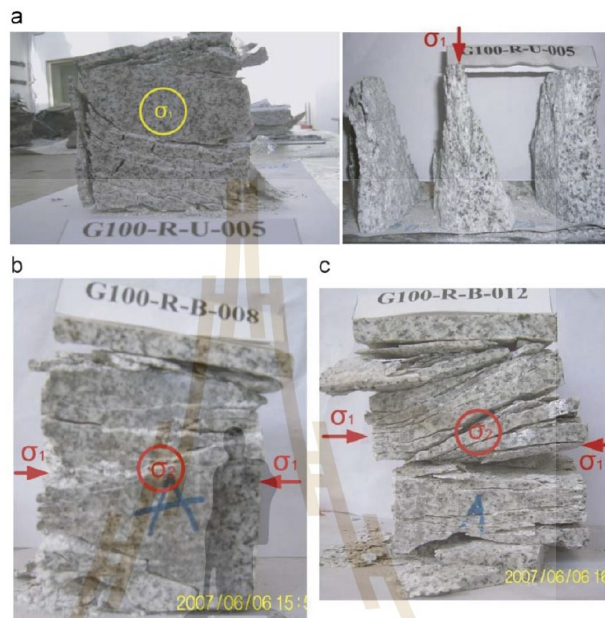
Figure 2.5   Spalling failure of granite: (a) uniaxial; (b) biaxial—loading path1; and (c) biaxial—loading path 2—under higher confinement (Yun et al., 2010)

Sagong et al. (2011) study rock fracture and behavior of jointed rock mass around boundary of tunnel were performed with an opening under biaxial compression through numerical analysis (PFC2D) and experiment. A rock-like model of 40 x 100 x 130 mm^3, a joint set was created with angles of 30°, 45°, and 60° to the horizontal, while a thickness 2 mm of the joint for acrylic plate. The opening has a diameter of 80 mm (figure 2.6). As a result, the progressive fracture behavior (Figure 2.7) when cracking propagation of tensile cracks in a low joint angle rock, for high joint angle rock cause develops into a removable block on rock specimen and rock model when there is an increase in the lower stress induce tensile fractures with a decrease joint angle but this is the opposite of the damage zone around the opening.

Figure 2.6   Jointed rock model (set dipping at 30°) (Sagong et al., 2011)
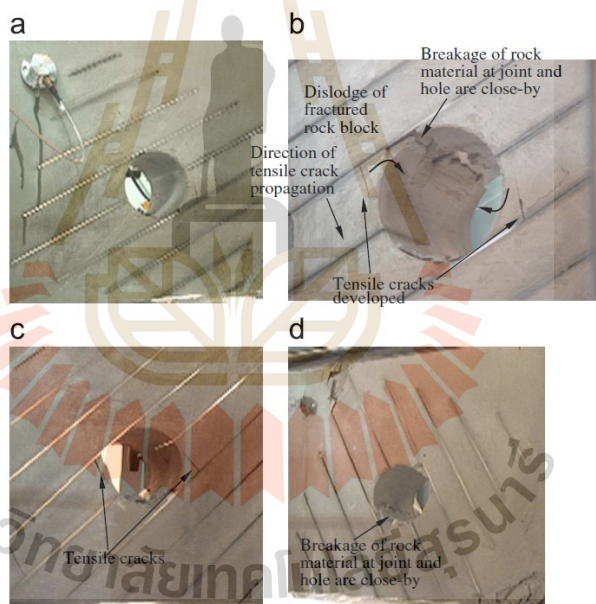
Figure 2.7   Rock fracture characteristics mode under biaxial loading
condition (Sagong et al., 2011)

Zhang et al. (2017) investigate mechanical behavior of rock under biaxial stress state, using a model to estimate the strength of rock as well as at the microscopic element level. The modified Wiebols-Cook criterion and Drucker-Prager criterion are applied to assess rock strength. An experiment to analyze failure behavior and the strength of coal under biaxial compression (Figure 2.8). The coal

specimen provides consistent results. Comparisons of the experimental results (Figure 2.9) with theoretical results were shown in stress-strain curve of brittle rock provided a good prediction under plane-strain and variations matched with under plane-strain biaxial stress state (PSBSS).
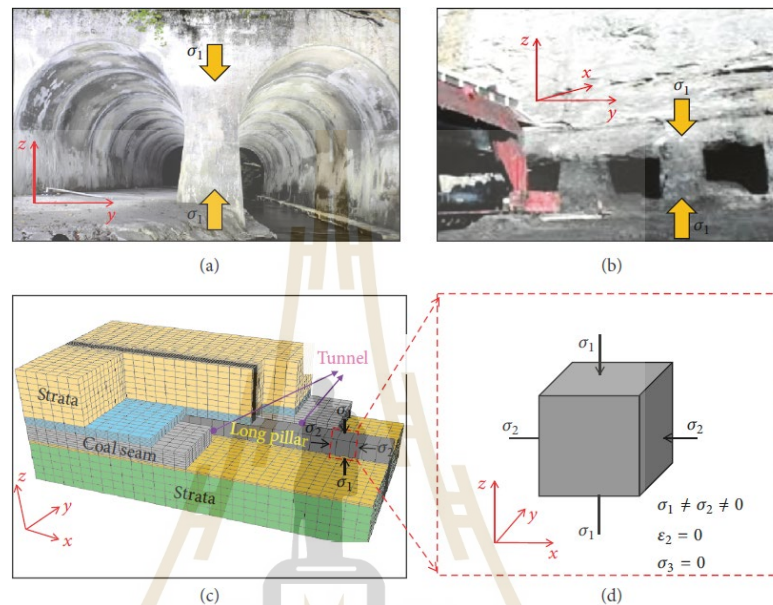
Figure 2.8   Pillars under PSBSS (a) Rock pillar between adjacent tunnels; (b) coal pillar in highwall mining; (c) coal pillar in longwall mining; (d) rock block under PSBSS (Zhang et al., 2017)
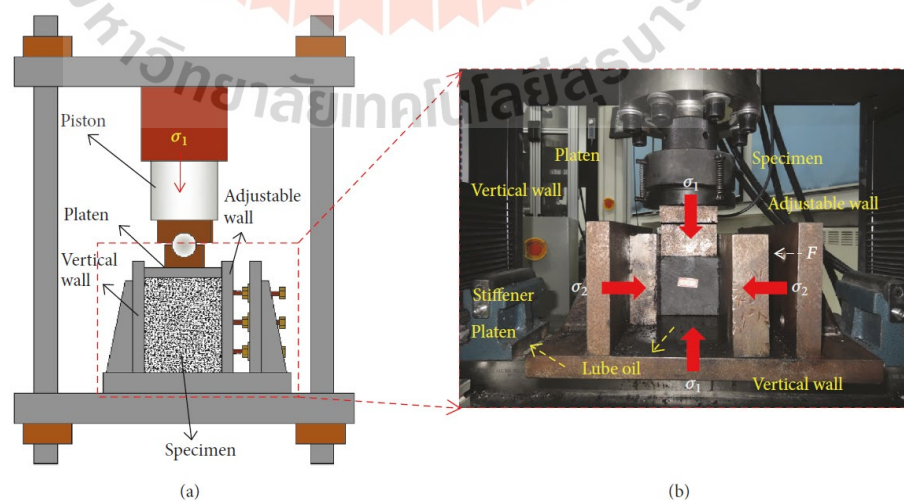
Figure 2.9   Biaxial compression test system (a) Schematic of test system; (b) The experimental set-up (Zhang et al., 2017)

Garg et al. (2018) study the failure mode of intact rock by the schematic of test system based on machine by Arora and Mishra, (2015) as shown in Figures 2.10 and 2.11 under biaxial test using Berea sandstone with cubic specimen 50.8 mm on all sides of the rock. As Mohr-Coulomb failure criteria and Hoek-Brown are not suitable for biaxial stress conditions, the Drucker-Prager failure criterion equation was used instead (Figure 2.12). The failure characteristics of the sandstone tested are separated from the center of the sample by shear with multiple intersecting shears, showing characteristics that are separated from the free surface by shear failure, where the severity is directly dependent on the intermediate stress is shown in Figure 2.13 and the uniaxial failure strength test is lower than the biaxial failure strength with every increase in confinement.
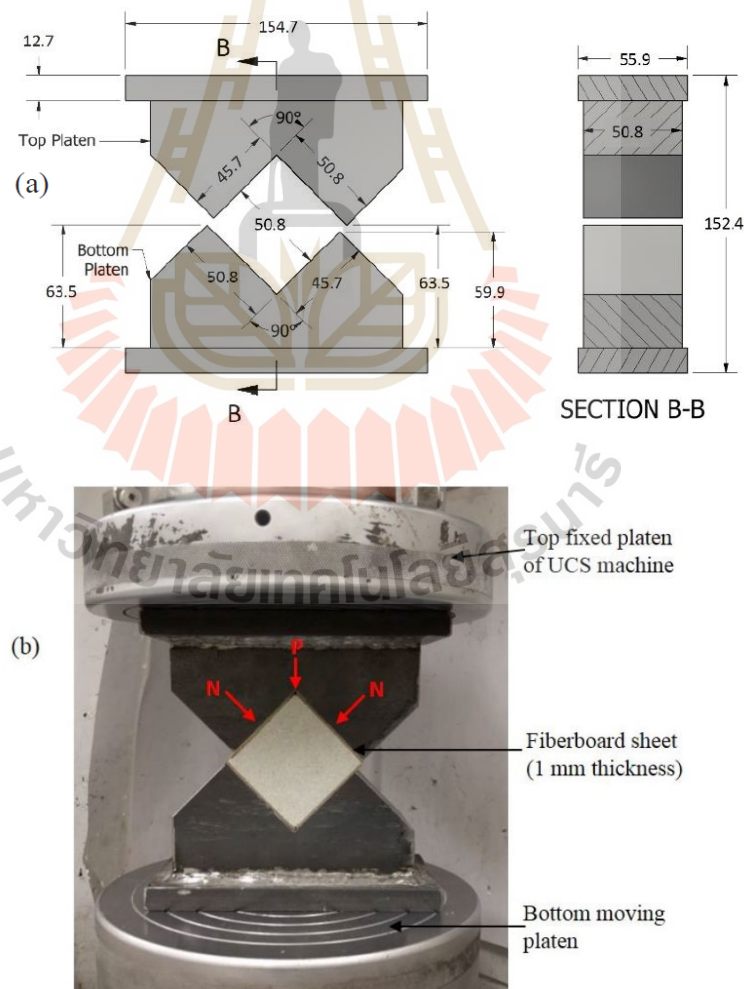
Figure 2.10   (a) Schematic diagram of biaxial test (Units: mm);

(b) Biaxial test setup (Arora and Mishra, 2015)
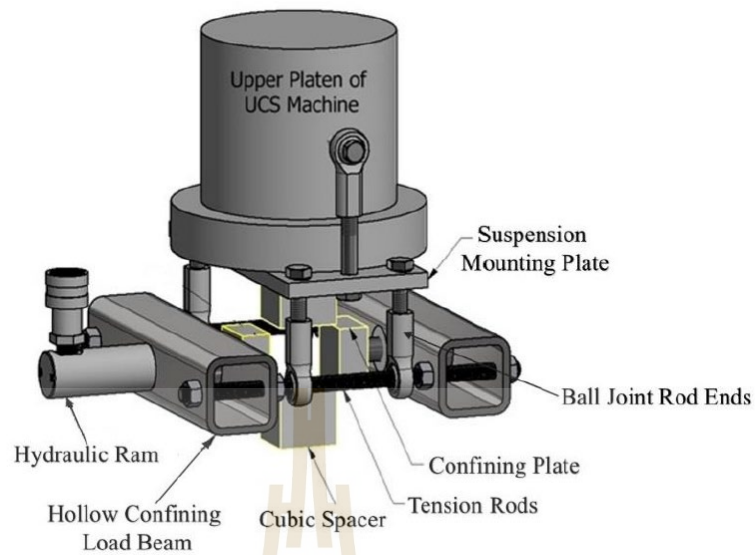
Figure 2.11   Schematic view of biaxial test with confining device (Garg et al., 2018)
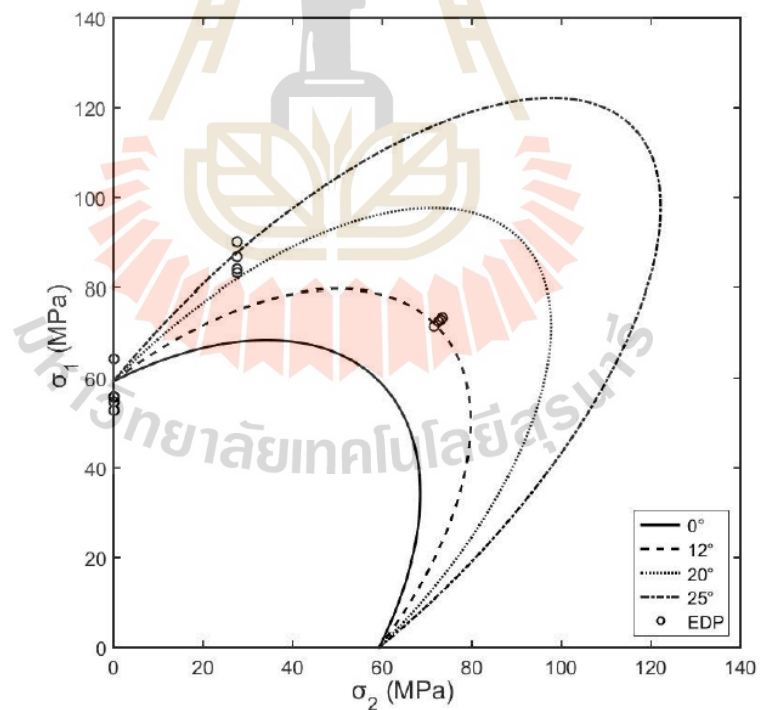
Figure 2.12 Drucker-Prager criteria with data points (EDP) at failure (Garg et al., 2018)
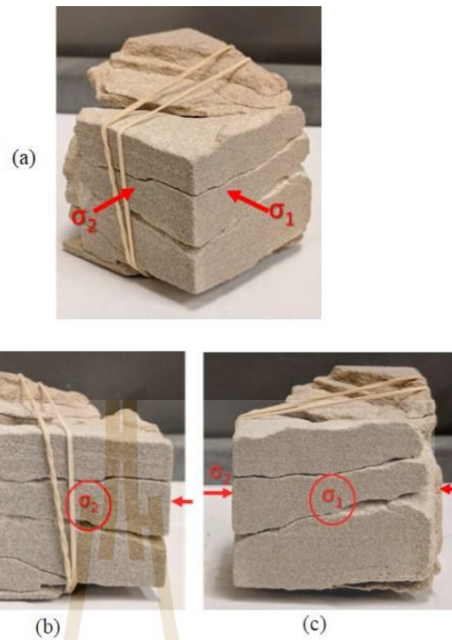
Figure 2.13   Failure mode of sandstone in biaxial test (a) Diagonal view;
(b) σ_1– σ_3 plane; (c) σ_2– σ_3 plane (Garg et al., 2018)

Liu et al. (2020) perform dynamic biaxial compression tests with cubic specimen of sandstone using a newly developed triaxial Hopkinson bar (Figure 2.14) to study rock behavior under biaxial static pre-stress (σ_1, σ_2) conditions, 0, 10, 20, 30 and 40 MPa, with impact velocity differences of 15, 20 and 26 m/s coincidings to average axial strain rates of 80, 200 and 250s-1. High-speed 3-D digital image correlation (3D-DIC) (Figure 2.15) and synchrotron-based micro-computed tomography (μCT) were used to analyze the level characteristics microstructure of rock to macroscopic. Results indicate that strength of specimen increases with strain rate and that the impact of velocity decreases when increasing pre-stress values (σ_1) along the impact direction and σ_2 also rise in the lateral direction. Rock ejection depends not only on dynamic input power and confining pre-stress also on rock properties. The μCT imaging techniques (Figure 2.16) explain that the failure angle depends on the same confining pressure as impact velocity. The increase in pre-stress σ_1 contributes to the spread of crack propagation and weakens the rock strength as opposed to effect of σ_2.

Figure 2.14   Triaxial Hopkinson bar (Liu et al., 2020)
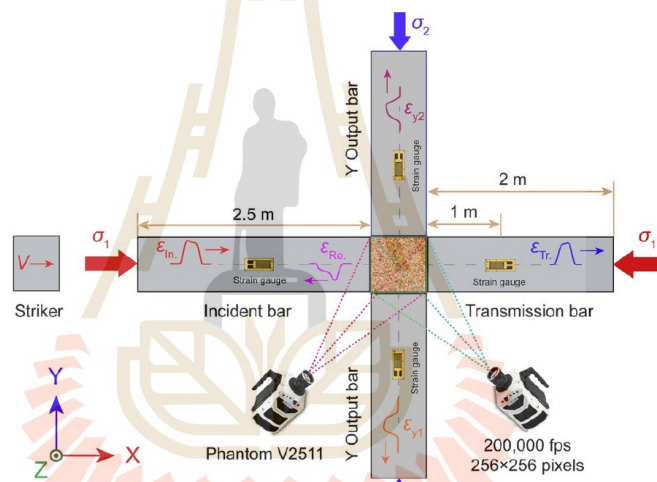
Figure 2.15 3D-DIC imaging set up (Liu et al., 2020)
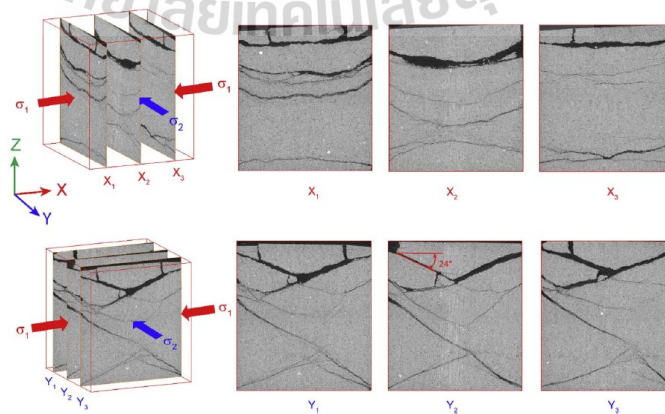
Figure 2.16   Tomographic cross-sections of sandstone specimen under

biaxial pre-stress condition of (20, 10) MPa. (Liu et al., 2020)

CHAPTER III

SAMPLE PREPARATION

This chapter describes rock sample preparation. The rock samples used in this study are commonly encountered in underground excavations in Thailand. They include Korat group (Phra Wihan sandstone, Phu Phan sandstone and Phu Kradung siltstone), Tak batholiths (granite), Lopburi formation (marble), Saraburi formation (limestone), and Nakhon Sawan formation (gypsum) in the northeastern Thailand. Table 3.1 shows the location and rock units from which they are obtained. Table 3.2 shows the mineral compositions of each rock. The cubic specimens are cut using high speed saw (Figure 3.1) to obtain a nominal dimension of 54×54×54 mm³, as shown in Figure 3.2. Five specimens have been prepared for each rock type. Sample preparation is carried out in the laboratory at Suranaree University of Technology. Table 3.3 summarizes the specimen number, dimensions and density.

Table 3.1 Rock samples

Rock Name	Density (g/cc)	Formation	Location
Granite	2.79 ± 0.03	Tak batholiths	Tak province
Limestone	2.63 ± 0.03	Lopburi	Lopburi province
Marble	2.65 ± 0.02	Saraburi	Saraburi province
Gypsum	2.16 ± 0.04	Nakhon Sawan	Nakhon Sawan province
Coarse grained sandstone	2.32 ± 0.01	Phu Phan	Nakhon Ratchasima province
Medium grained sandstone	2.31 ± 0.03		
Fine grained sandstone	2.26 ± 0.07		
Fine grained sandstone	2.24 ± 0.03	Phra Wihan	
Siltstone	2.48 ± 0.01	Phu Kradung	

Table 3.2 Mineral compositions of rock (Khamrat et al., 2016)

Rock Name	Mineral compositions and crystal/grain sizes (in mm)
Granite	45% plagioclase (0.5–1 mm), 35% quartz (2–5 mm), 8% orthoclase (3–5 mm), 3% amphibole (1–2 mm), 2% biotite (1–2 mm) 7% other (0.5–1 mm)
Limestone	85% calcite (0.3–1.0 mm), 15% dolomite (0.5–1.2 mm)
Marble	100% calcite (1–2 mm)
Gypsum	100% gypsum (0.5-1 mm)
Coarse grained (Phu Phan)	70% quartz (0.5–2 mm), 20% feldspar (0.2–0.5 mm), 7% mica (0.1–0.5 mm), 3% lithic fragment (0.1–1 mm)
Medium grained (Phu Phan) sandstone	72% quartz (0.25–0.5 mm), 15% feldspar (0.2–0.5 mm), 8% mica (0.1–0.5 mm), 5% lithic fragment (0.1–1 mm)
Fine grained (Phu Phan) sandstone	68% quartz (0.06–0.25 mm), 22% feldspar (0.1–0.8 mm), 5% mica (0.1–0.3 mm), 3% rock fragment (0.5–2 mm), 2% other (0.5–1 mm)
Fine grained (Phra Wihan) sandstone	66% quartz (0.06–0.25 mm), 20% feldspar (0.1–0.8 mm), 5% mica (0.1–0.3 mm), 5% rock fragment (0.5–2 mm), 4% other (0.5–1 mm)
Siltstone	70% lithic fragment (0.1–0.3 mm), 18% quartz (0.1–0.5 mm), 7% mica (0.1–0.5 mm), 3% feldspar (0.1–0.5 mm), 2% other (0.1–0.8 mm)

Figure 3.1 High speed saw to cut rock samples

Figure 3.2   Rock specimens prepared for uniaxial and biaxial testing

Table 3.3 Specimen dimensions

Rock Name	Specimen No.	Length (mm)	Width (mm)	Height (mm)	Density (g/cc)
Granite	GR-UCS-01	51.50	47.00	47.00	2.81
	GR-BI-02	51.12	47.00	47.00	2.83
	GR-BI-03	53.00	47.00	47.00	2.79
	GR-BI-04	54.00	47.00	47.00	2.81
	GR-BI-05	54.98	47.00	47.00	2.73
Average					2.79 ± 0.03
Limestone	LS-UCS-01	52.96	52.38	53.02	2.66
	LS-BI-02	54.02	53.34	53.80	2.63
	LS-BI-03	50.50	52.08	54.18	2.67
	LS-BI-04	53.30	52.16	53.00	2.64
	LS-BI-05	53.80	53.24	53.42	2.63
Average					2.65 ± 0.02
Marble	MB-UCS-01	54.12	54.06	54.98	2.67
	MB-BI-02	54.58	54.76	54.16	2.62
	MB-BI-03	53.82	53.40	53.56	2.59
	MB-BI-04	53.62	53.54	53.84	2.64
	MB-BI-05	54.98	55.00	54.58	2.61
Average					2.63 ± 0.03
Gypsum	GYP-UCS-01	51.50	53.52	53.90	2.15
	GYP-BI-02	51.12	53.94	53.44	2.17
	GYP-BI-03	53.00	53.26	52.74	2.19
	GYP-BI-04	54.00	52.76	53.70	2.19
	GYP-BI-05	54.98	53.04	54.62	2.08
Average					2.16 ± 0.04
Coarse grained (Phu Phan) sandstone	S1-UCS-01	54.36	53.76	54.34	2.32
	S1-BI-02	53.90	54.22	52.76	2.31
	S1-BI-03	53.24	54.98	54.72	2.31
	S1-BI-04	53.40	54.43	54.52	2.34
	S1-BI-05	54.16	53.42	54.56	2.32
Average					2.32 ± 0.01

Table 3.3 Specimen dimensions

Rock Name	Specimen No.	Length (mm)	Width (mm)	Height (mm)	Density (g/cc)
Medium grained (Phu Phan) sandstone	S2-UCS-01	54.72	54.32	54.62	2.31
	S2-BI-02	55.10	54.82	55.18	2.31
	S2-BI-03	53.80	53.36	53.94	2.29
	S2-BI-04	54.16	53.90	55.06	2.28
	S2-BI-05	53.50	54.16	54.30	2.35
Average					2.31 ± 0.03
Fine grained (Phu Phan) sandstone	S3-UCS-01	51.50	47.00	47.00	2.81
	S3-BI-02	51.12	47.00	47.00	2.83
	S3-BI-03	53.00	47.00	47.00	2.79
	S3-BI-04	54.00	47.00	47.00	2.81
	S3-BI-05	54.98	47.00	47.00	2.73
Average					2.26 ± 0.07
Fine grained (Phra Wihan) sandstone	S4-UCS-01	51.50	53.52	53.90	2.25
	S4-BI-02	51.12	53.94	53.44	2.37
	S4-BI-03	53.00	53.26	52.74	2.20
	S4-BI-04	54.00	52.76	53.70	2.30
	S4-BI-05	54.98	53.04	54.62	2.16
Average					2.24 ± 0.03
Siltstone	ST-UCS-01	54.56	53.46	53.86	2.21
	ST-BI-02	53.64	54.02	54.20	2.22
	ST-BI-03	53.20	53.14	53.96	2.28
	ST-BI-04	53.78	53.16	53.44	2.23
	ST-BI-05	54.02	53.94	53.44	2.27
Average					2.48 ± 0.01

CHAPTER IV

TEST METHOD

4.1 Introduction

This chapter describes the testing equipment, methods, and calculation of rock strength and elastic parameters for the biaxial compression test.

4.2 Test equipment

The main equipment for the uniaxial and biaxial compression tests is the true triaxial loading frame (Fuenkajorn et al., 2012), as shown in Figure 4.1. This device is used to obtain the biaxial compressive strengths and elastic parameters of rock specimens with soft to medium strengths. It has been used to apply axial stress (σ_1) and lateral stress (σ_2) on rock specimens. The frame comprises four main components; three mutually perpendicular steel load frames to secure rock specimens in the center, hydraulic cylinders, a measurement system, and two hydraulic pumps. The measurement system includes pressure gages and dial gages.

The test procedure and calculation follow the ASTM D7012-14 standard except for the shape of the rock specimens. This device can test cubic or rectangular specimens by adjusting the distances between the opposite steel loading platens. For all tests, neoprene sheets are placed at all interfaces between the loading platens and specimen surfaces to minimize friction.

4.3 Test method

All tests have used the Lode parameter (L) to describe stress state. Lode (1926) parameter describes test conditions, L=1 for compression, 1<L<-1 for polyaxial loading, and L=-1 for extension loading where Lode parameter can be calculated as follows:

$$L = \frac{2\sigma_2 - \sigma_3 - \sigma_1}{\sigma_3 - \sigma_1} \qquad (4.1)$$
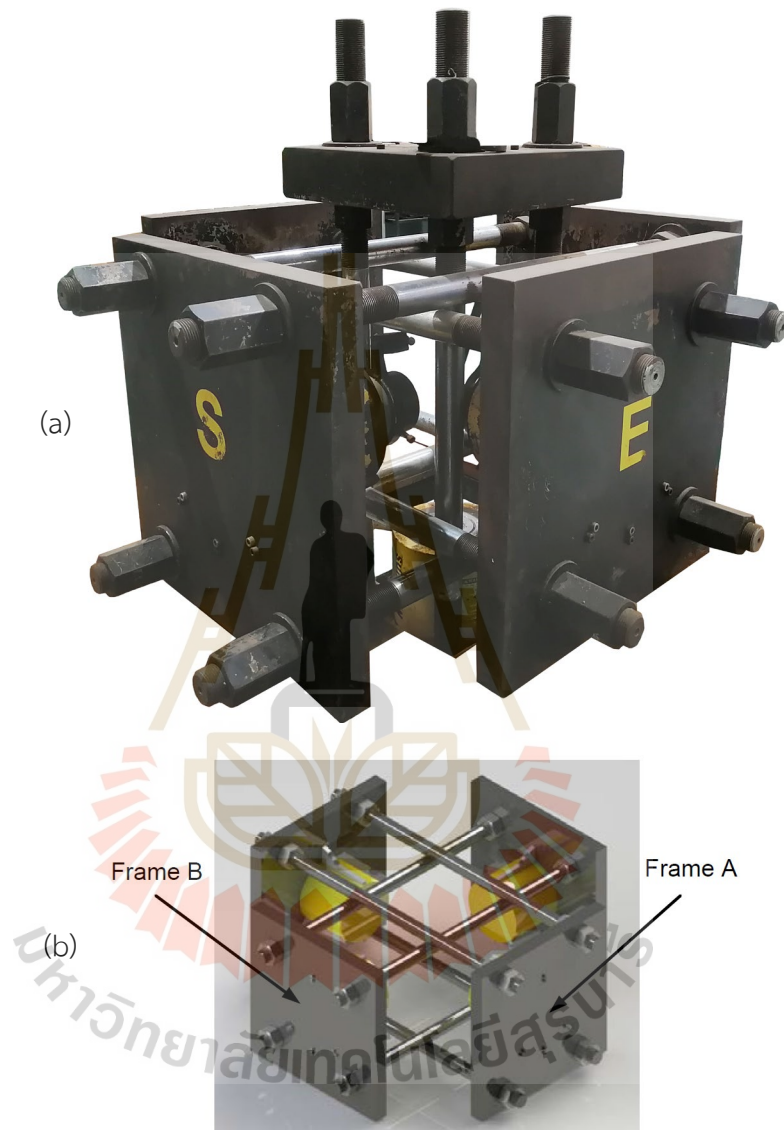
Figure 4.1 True triaxial loading frame (a) and two steel cross load frames (b)
(Fuenkajorn et al., 2012)

From Figure 4.2, the red dash line (L=1) shows the test scheme by increasing σ_1 while σ_2 and σ_3 are maintained constant at zero, i.e., to obtain strength under uniaxial compression.

The biaxial compression ($\sigma_1 = \sigma_2$) or biaxial test is performed by that the maximum (σ_1) and intermediate (σ_2) principal stresses are equally increased until failure occurs while σ_3 is maintained at zero.

The intermediate principal stress (σ_2) can be calculated in according to Table 4.1. Finding the value of σ_2 for L=0, 0.5, and -0.5 can be achieved from quotient of the sum of failure stress (σ_1) between uniaxial (L=1) and biaxial compression (L=-1), σ_1 between L=1 and L=0, and σ_1 between L=0 and L=-1, respectively. They can be calculated as:

For L=0,

$$(\sigma_{1, L=-1} + \sigma_{1, L=1})/2, \text{ or } 0.5(\sigma_{1, L=-1}) \tag{4.2}$$

For L=0.5,

$$(\sigma_{1, L=0} + \sigma_{1, L=1})/2, \text{ or } 0.25(\sigma_{1, L=-1}) \tag{4.3}$$

For L=-0.5,

$$(\sigma_{1, L=-1} + \sigma_{1, L=0})/2, \text{ or } 0.75(\sigma_{1, L=-1}) \tag{4.4}$$

For all tests σ_1 is increased at a rate of 0.1 MPa/s.

Figure 4.2 and Table 4.1 describe the test plan. Neoprene sheets are placed at all interfaces between the loading platens and specimen surfaces. Deformations are measured to the nearest ± 10 microns.

4.4 Calculations of elastic parameters

Assuming that the specimens are linearly elastic and isotropic, the stress-strain components show linear relation which can be represented by the principal stresses (σ_1, σ_2, σ_3) and principal strains (ε_1, ε_2, ε_3). The λ and G are constants called Lame's

parameters and shear modulus. E and Poisson's ratio (ν) can be determined by Brady and Brown (2007), as follows:

$$\sigma_1 = \lambda\,(\varepsilon_1 + \varepsilon_2 + \varepsilon_3) + 2G\varepsilon_1 \tag{4.5}$$

$$\sigma_2 = \lambda\,(\varepsilon_1 + \varepsilon_2 + \varepsilon_3) + 2G\varepsilon_2 \tag{4.6}$$
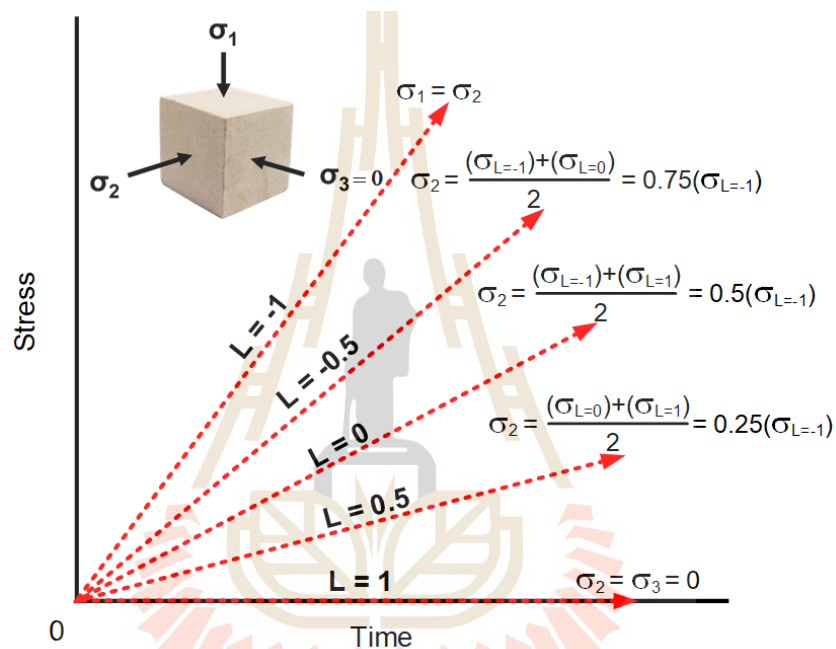
Figure 4.2 Loading paths for biaxial testing

Table 4.1 Test sequence

Test sequence	Lode Parameter (L)	σ_2 (MPa)
1	1 (Uniaxial)	0
2	-1 (Biaxial)	$\sigma_1 = \sigma_2$
3	0	$(\sigma_{1,\,L=-1} + \sigma_{1,\,L=1})/2$ or $0.5(\sigma_{1,\,L=-1})$
4	0.5	$(\sigma_{1,\,L=0} + \sigma_{1,\,L=1})/2$ or $0.25(\sigma_{1,\,L=-1})$
5	-0.5	$(\sigma_{1,\,L=-1} + \sigma_{1,\,L=0})/2$ or $0.75(\sigma_{1,\,L=-1})$

Subtracting equations (4.5) from (4.6):

$$\sigma_1 - \sigma_2 = 2G\,(\varepsilon_1 - \varepsilon_2) \tag{4.7}$$

By substituting σ_1, σ_2, ε_1, and ε_2 in equation (4.7), G can be obtained. Substituting G into equation (4.5) or (4.6) to get λ value. The proportion between λ and G is used to find Poisson's ratio (ν), as follow:

$$\frac{\lambda}{G} = \frac{2\nu}{1-2\nu} \tag{4.8}$$

The elastic modulus (E) can be obtained from:

$$E = 2G\,(1+\nu) \tag{4.9}$$
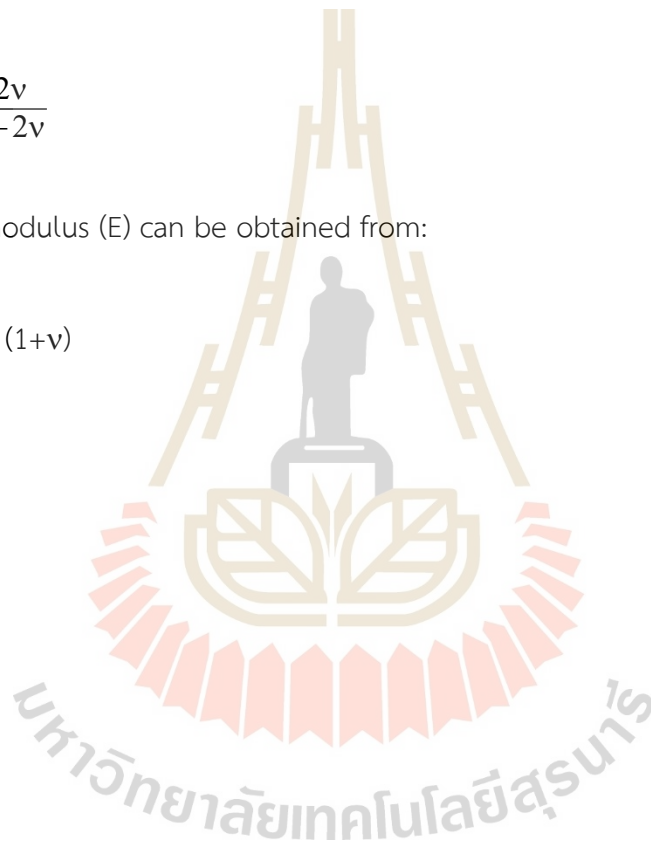
CHAPTER V

TEST RESULTS

5.1 Test results

This section describes test results in terms of rock strength and elasticity. The deformations determine the strains along the principal axes during loading. Appendix A shows the stress-strain curves.

5.1.1 Strength results

Figure 5.1 gives examples of stress-strain curves obtained from the biaxial compression test of granite. The diagrams show that ε_1 is axial strain, ε_2 and ε_3 are lateral strains, and ε_v is volumetric strain. The uniaxial test gives dilation of ε_2 and ε_3 with similar expansion values. For the biaxial test, the lateral strains extend unequally due to σ_2 resulting in less dilatation of ε_2 but ε_3 is greater due to free surface as minimum stress (σ_3) equal zero. This holds true for all tested rocks.

The calculated strengths of all tested rocks are shown in Figure 5.2 and their numerical values are given in Table 5.1. Granite shows highest compressive strengths while gypsum shows the lowest values. All rock types exhibit similar evolution of the strengths ($\sigma_{1,f}$) with the change of intermediate principal stress (σ_2). The results show rock strengths of the biaxial test are always higher than the uniaxial test.

The strengths initially increase with increasing σ_2 or with decreasing Lode parameters (L). The maximum strengths are reached at the Lode parameter of about -0.5. Below L = -0.5, the major principal stress at failure decreases. This occurs for all rock types.

Stress-strain curves and strengths show the intermediate principal stress (σ_2) effects on failure stresses which tend to be more pronounced under high σ_2. These observations agree with those obtained elsewhere (e.g., Colmenares and Zoback, 2002 and Haimson, 2006).
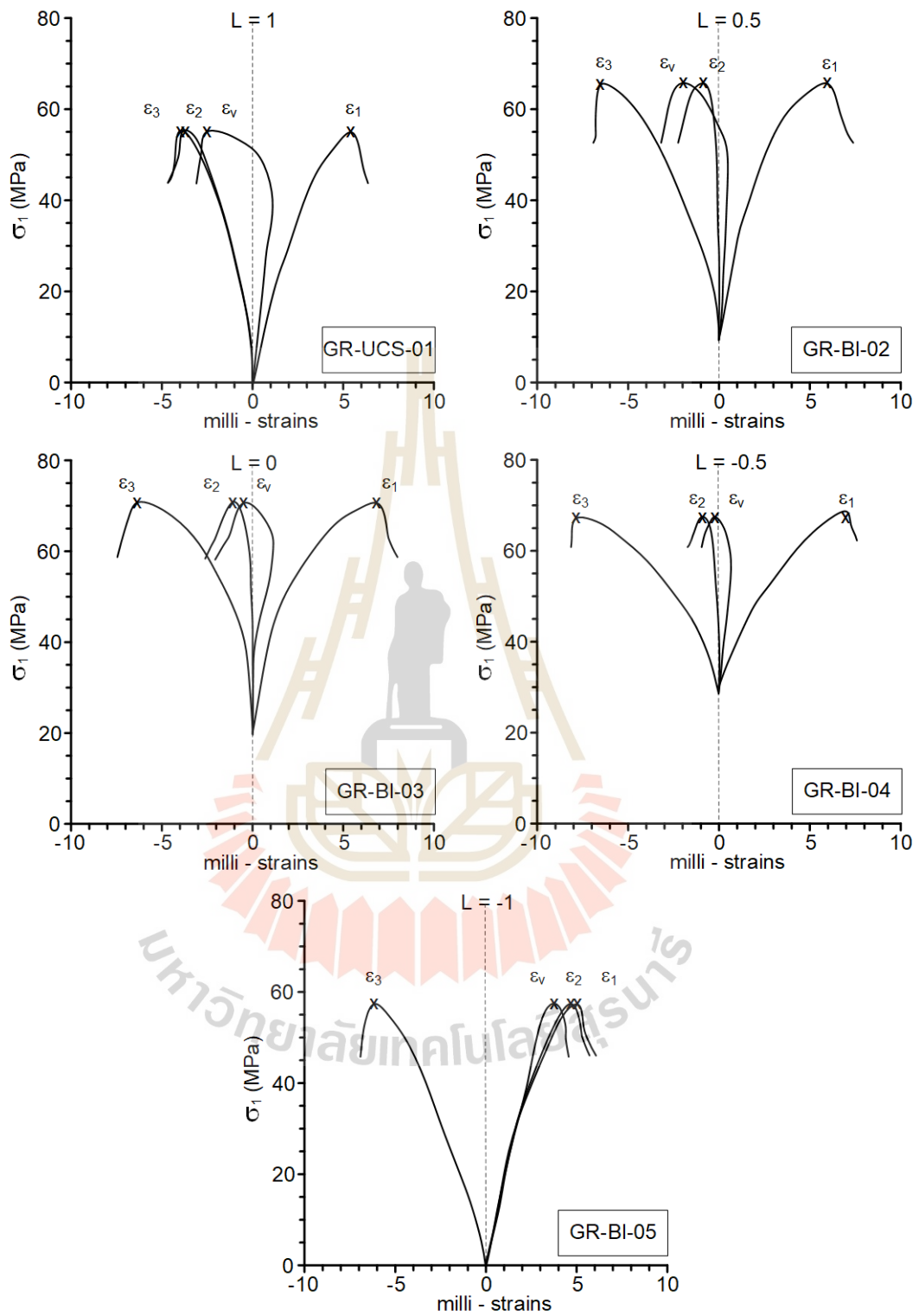
Figure 5.1 Examples of stress-strain curves of granite under various Lode parameters
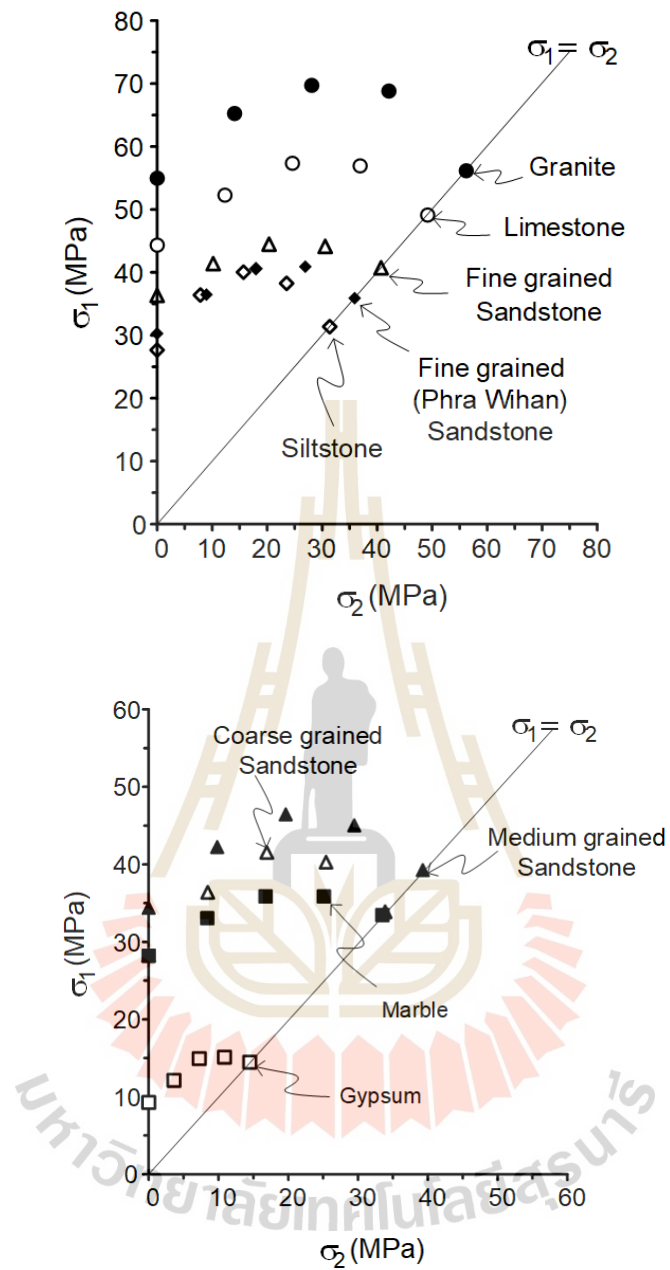
Figure 5.2 Failure stress (σ_1) and intermediate stress (σ_2)

of all tested rocks in σ_1–σ_2 diagrams

Table 5.1 Summary of rock strengths

Rock Name	Specimen No.	Lode parameter (L)	Failure stresses		
			σ_1 (MPa)	σ_2 (MPa)	σ_m (MPa)
Granite	GR-UCS-01	1.0	54.98	0.00	18.33
	GR-BI-02	0.5	65.27	14.04	26.44
	GR-BI-03	0.0	69.73	28.08	32.60
	GR-BI-04	-0.5	68.83	42.13	36.98
	GR-BI-05	-1.0	56.17	56.17	37.45
Limestone	LS-UCS-01	1.0	44.36	0.00	14.79
	LS-BI-02	0.5	52.29	12.29	21.53
	LS-BI-03	0.0	57.37	24.58	27.31
	LS-BI-04	-0.5	56.95	36.87	31.27
	LS-BI-05	-1.0	49.16	49.16	32.77
Marble	MB-UCS-01	1.0	28.22	0.00	9.41
	MB-BI-02	0.5	33.06	8.37	13.81
	MB-BI-03	0.0	35.87	16.74	17.54
	MB-BI-04	-0.5	35.86	25.11	20.32
	MB-BI-05	-1.0	33.47	33.47	22.32
Gypsum	GYP-UCS-01	1.0	9.28	0.00	3.09
	GYP-BI-02	0.5	12.13	3.62	5.25
	GYP-BI-03	0.0	14.93	7.24	7.39
	GYP-BI-04	-0.5	15.11	10.86	8.66
	GYP-BI-05	-1.0	14.48	14.48	9.65
Coarse grained (Phu Phan) sandstone	S1-UCS-01	1.0	34.40	0.00	11.47
	S1-BI-02	0.5	42.25	9.82	17.36
	S1-BI-03	0.0	46.47	19.64	22.04
	S1-BI-04	-0.5	45.05	29.46	24.84
	S1-BI-05	-1.0	39.27	39.27	26.18

Table 5.1 Summary of rock strengths

Rock Name	Specimen No.	Lode parameter (L)	Failure stresses		
			σ_1 (MPa)	σ_2 (MPa)	σ_m (MPa)
Medium grained (Phu Phan) sandstone	S2-UCS-01	1.0	28.27	0.00	9.42
	S2-BI-02	0.5	36.40	8.47	14.95
	S2-BI-03	0.0	41.55	16.94	19.50
	S2-BI-04	-0.5	40.28	25.40	21.89
	S2-BI-05	-1.0	33.87	33.87	22.58
Fine grained (Phu Phan) sandstone	S3-UCS-01	1.0	36.35	0.00	12.12
	S3-BI-02	0.5	41.38	10.18	17.19
	S3-BI-03	0.0	44.48	20.36	21.61
	S3-BI-04	-0.5	44.13	30.54	24.89
	S3-BI-05	-1.0	40.72	40.72	27.15
Fine grained (Phra Wihan) sandstone	S4-UCS-01	1.0	30.30	0.00	10.10
	S4-BI-02	0.5	36.47	8.98	15.15
	S4-BI-03	0.0	40.61	17.95	19.52
	S4-BI-04	-0.5	40.91	26.93	22.61
	S4-BI-05	-1.0	35.91	35.91	23.94
Siltstone	ST-UCS-01	1.0	27.66	0.00	9.22
	ST-BI-02	0.5	36.43	7.85	14.76
	ST-BI-03	0.0	40.05	15.69	18.58
	ST-BI-04	-0.5	38.27	23.54	20.60
	ST-BI-05	-1.0	31.39	31.39	20.93

5.1.2 Mode of Failures

Post-test failure appearance show that compressive shear failures are predominant in the specimens tested under low σ_2 while splitting tensile fractures parallel to σ_1 and σ_2 directions dominate under higher σ_2. It can explain that increase of σ_2 or decrease of L induces multiple extensile fractures on the specimens. These fractures are parallel to the σ_1-σ_2 plane. The larger σ_2 values are applied, the greater numbers of the extensile fractures are obtained. These modes of failure can be observed more clear for strong rocks (such as granite and limestone), as compared to the softer rocks, as shown in Figure 5.3. Under low σ_2 values, combination of shear failure and extensile fractures are observed. Table 5.2 summarizes mode of failure for each test scheme.

Under the conditions of all biaxial tests, the observed multiple extensile fractures under relatively high σ_2 suggest that the fracture initiation has no influence at the loading interface in the σ_2 direction. As a result, increase of σ_1 with σ_2 get the interface in the σ_2 direction contributes to the increase of σ_1 at failure.

5.1.3 Results of Elastic parameters

The elastic parameters for the nine rock types tend to be independent of the changes of intermediate principal stress and Lode parameter. For each rock type, small variations of E and ν are observed. This may be due to the intrinsic variability of the rocks. Figures 5.4 and 5.5 plot the elastic modulus and Poisson's ratios as a function of Lode parameter for all rock types. Their numerical values are given in Table 5.3.

Granite

σ_1

σ_2 σ_3

Limestone

Marble

Gypsum

Coarsed grained sandstone

Medium grained sandstone

Fine grained sandstone

Fine grained (Phra Wihan) sandstone

Siltstone

| L = 1 | L = 0.5 | L = 0 | L = -0.5 | L = -1 |
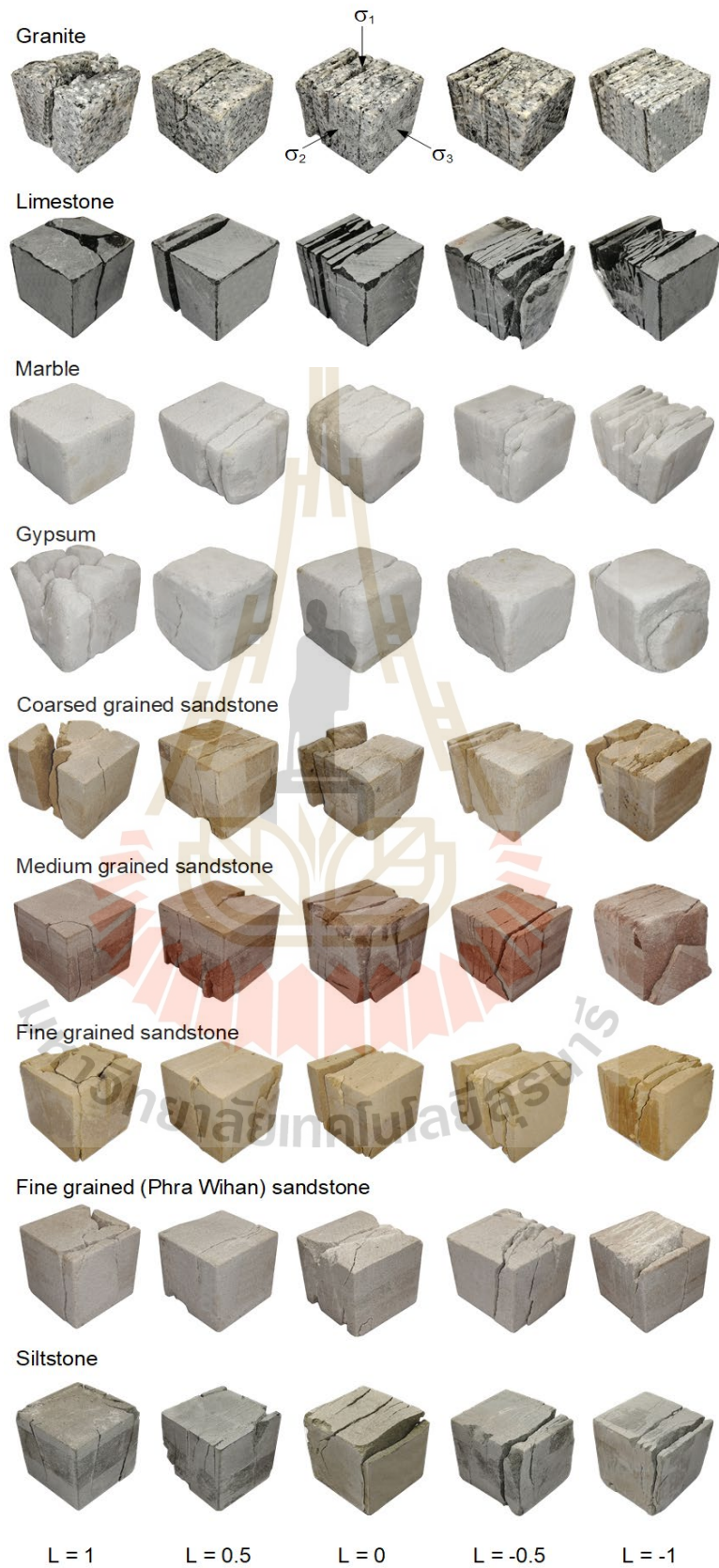
Figure 5.3 Post-test specimens

Table 5.2 Summary of modes of failure

Rock Name	Specimen No.	Lode parameter (L)	Mode of failure
Granite	GR-UCS-01	1.0	Single shear plane
	GR-BI-02	0.5	Multiple extensile plane
	GR-BI-03	0.0	Multiple extensile plane
	GR-BI-04	-0.5	Multiple extensile plane
	GR-BI-05	-1.0	Multiple extensile plane
Limestone	LS-UCS-01	1.0	Single shear plane
	LS-BI-02	0.5	Multiple extensile plane
	LS-BI-03	0.0	Multiple extensile plane
	LS-BI-04	-0.5	Multiple extensile plane
	LS-BI-05	-1.0	Multiple extensile plane
Marble	MB-UCS-01	1.0	Single shear plane
	MB-BI-02	0.5	Multiple extensile plane
	MB-BI-03	0.0	Multiple extensile plane
	MB-BI-04	-0.5	Multiple extensile plane
	MB-BI-05	-1.0	Multiple extensile plane
Gypsum	GYP-UCS-01	1.0	Single shear plane
	GYP-BI-02	0.5	Multiple extensile plane
	GYP-BI-03	0.0	Multiple extensile plane
	GYP-BI-04	-0.5	Multiple extensile plane
	GYP-BI-05	-1.0	Multiple extensile plane
Coarse grained (Phu Phan) sandstone	S1-UCS-01	1.0	Single shear plane
	S1-BI-02	0.5	Multiple extensile plane
	S1-BI-03	0.0	Multiple extensile plane
	S1-BI-04	-0.5	Multiple extensile plane
	S1-BI-05	-1.0	Multiple extensile plane

Table 5.2 Summary of modes of failure

Rock Name	Specimen No.	Lode parameter (L)	Mode of failure
Medium grained (Phu Phan) sandstone	S2-UCS-01	1.0	Single shear plane
	S2-BI-02	0.5	Multiple extensile plane
	S2-BI-03	0.0	Multiple extensile plane
	S2-BI-04	-0.5	Multiple extensile plane
	S2-BI-05	-1.0	Multiple extensile plane
Fine grained (Phu Phan) sandstone	S3-UCS-01	1.0	Single shear plane
	S3-BI-02	0.5	Multiple extensile plane
	S3-BI-03	0.0	Multiple extensile plane
	S3-BI-04	-0.5	Multiple extensile plane
	S3-BI-05	-1.0	Multiple extensile plane
Fine grained (Phra Wihan) sandstone	S4-UCS-01	1.0	Single shear plane
	S4-BI-02	0.5	Multiple extensile plane
	S4-BI-03	0.0	Multiple extensile plane
	S4-BI-04	-0.5	Multiple extensile plane
	S4-BI-05	-1.0	Multiple extensile plane
Siltstone	ST-UCS-01	1.0	Single shear plane
	ST-BI-02	0.5	Multiple extensile plane
	ST-BI-03	0.0	Multiple extensile plane
	ST-BI-04	-0.5	Multiple extensile plane
	ST-BI-05	-1.0	Multiple extensile plane
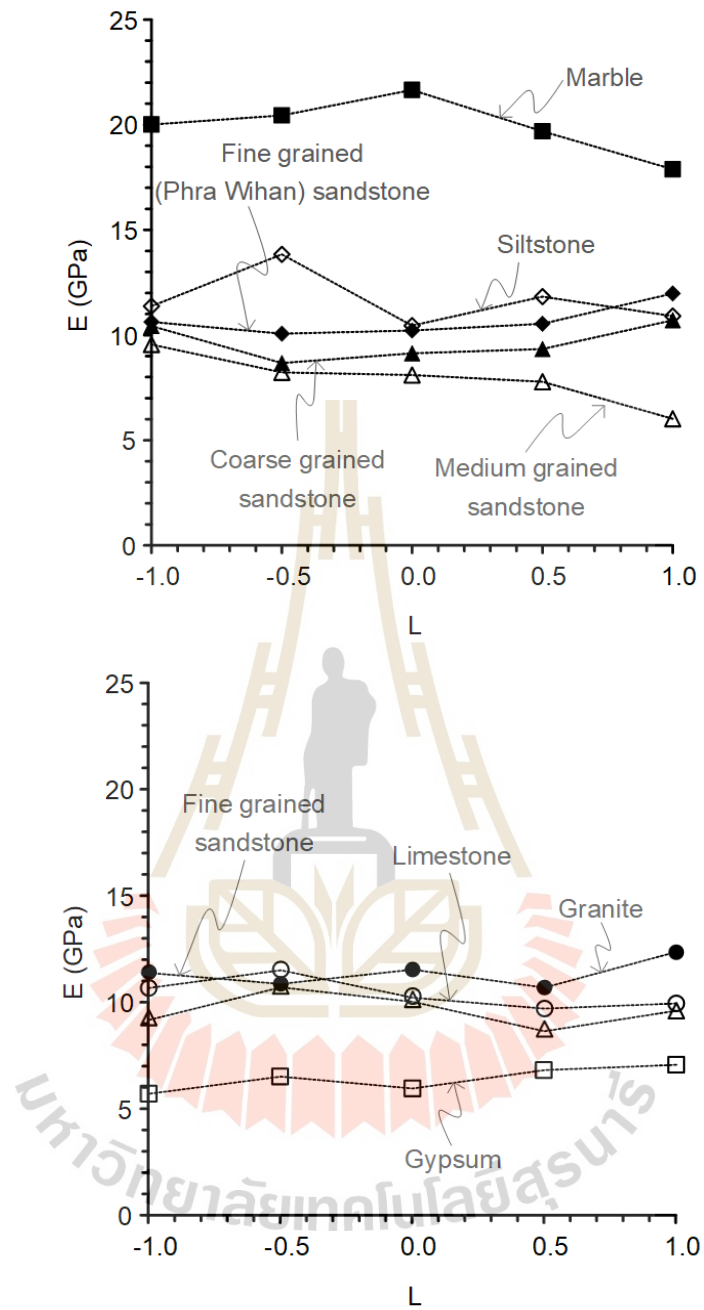
Figure 5.4 Elastic moduli as a function of Lode parameter
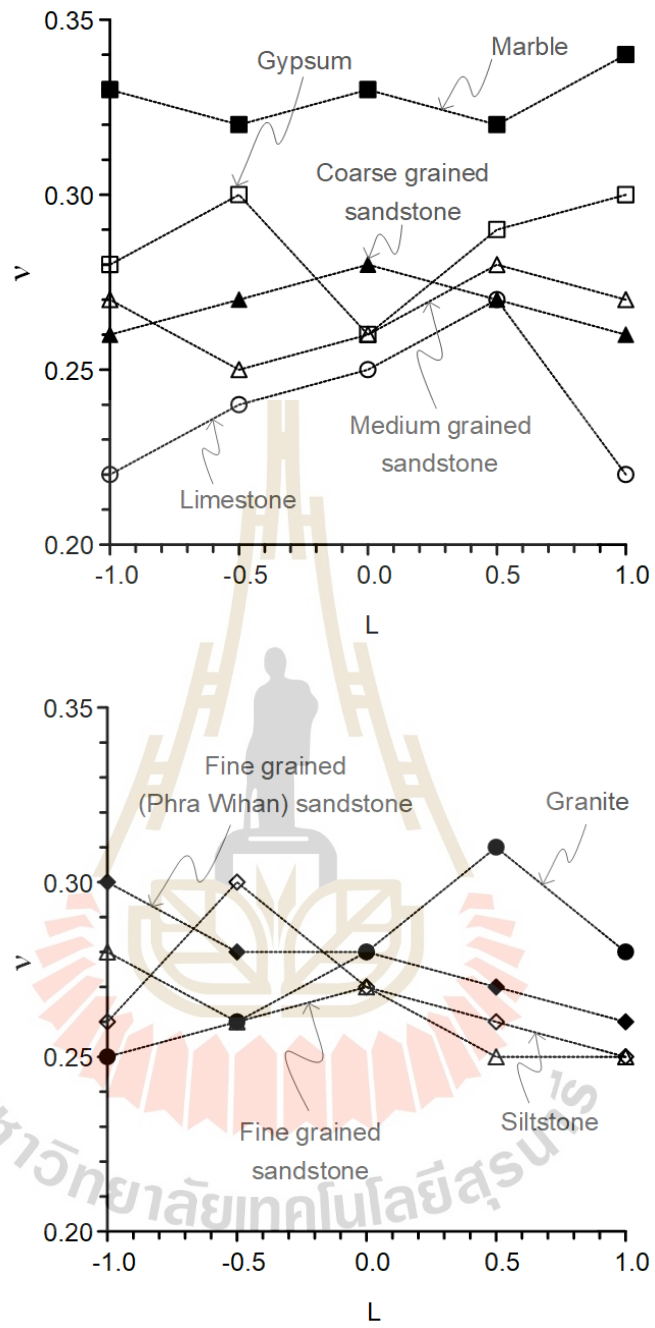
Figure 5.5 Poisson's ratios as a function of Lode parameter

Table 5.3 Summary of elastic parameters

Rock Name	Specimen No.	Lode parameter (L)	E (MPa)	ν	G (GPa)	λ (GPa)
Granite	GR-UCS-01	1.0	12.57	0.28	4.91	6.25
	GR-BI-02	0.5	11.10	0.30	4.27	6.4
	GR-BI-03	0.0	13.47	0.29	5.22	7.21
	GR-BI-04	-0.5	13.01	0.23	4.93	8.76
	GR-BI-05	-1.0	10.26	0.24	4.14	3.82
Average ± SD			12.08 ± 1.35	0.27 ± 0.03	4.69 ± 0.47	6.49 ± 1.79
Limestone	LS-UCS-01	1.0	9.80	0.22	4.02	3.16
	LS-BI-02	0.5	10.00	0.26	3.97	4.30
	LS-BI-03	0.0	10.50	0.26	4.17	4.52
	LS-BI-04	-0.5	12.01	0.23	4.88	4.16
	LS-BI-05	-1.0	11.87	0..20	4.94	3.30
Average ± SD			10.84 ± 1.04	0.24 ± 0.02	4.40 ± 0.48	3.89 ± 0.62
Marble	MB-UCS-01	1.0	17.88	0.34	6.67	14.18
	MB-BI-02	0.5	19.69	0.30	7.57	11.36
	MB-BI-03	0.0	21.65	0.35	8.02	18.71
	MB-BI-04	-0.5	19.89	0.33	7.48	14.51
	MB-BI-05	-1.0	20.68	0.31	7.89	12.88
Average ± SD			19.96 ± 1.39	0.33 ± 0.02	7.53 ± 0.53	14.33 ± 2.75
Gypsum	GYP-UCS-01	1.0	6.50	0.30	2.50	3.75
	GYP-BI-02	0.5	5.35	0.28	2.09	2.66
	GYP-BI-03	0.0	5.45	0.27	2.15	2.52
	GYP-BI-04	-0.5	5.61	0.31	2.14	3.49
	GYP-BI-05	-1.0	5.85	0.30	2.25	3.38
Average ± SD			5.75 ± 0.46	0.29 ± 0.02	2.23 ± 0.16	3.16 ± 0.54

Table 5.3 Summary of elastic parameters

Rock Name	Specimen No.	Lode parameter (L)	E (MPa)	ν	G (GPa)	λ (GPa)
Coarse grained (Phu Phan) sandstone	S1-UCS-01	1.0	10.70	0.26	4.26	4.62
	S1-BI-02	0.5	8.50	0.26	3.38	3.66
	S1-BI-03	0.0	9.00	0.28	3.52	4.47
	S1-BI-04	-0.5	8.70	0.27	3.44	4.04
	S1-BI-05	-1.0	10.50	0.25	4.20	4.20
Average ± SD			9.48 ± 1.04	0.26 ± 0.01	3.76 ± 0.43	4.20 ± 0.38
Medium grained (Phu Phan) sandstone	S2-UCS-01	1.0	6.02	0.26	2.39	2.59
	S2-BI-02	0.5	7.11	0.26	2.82	3.06
	S2-BI-03	0.0	8.20	0.27	3.25	3.81
	S2-BI-04	-0.5	7.80	0.28	3.05	3.88
	S2-BI-05	-1.0	10.10	0.27	3.98	4.67
Average ± SD			7.85 ± 1.51	0.27 ± 0.01	3.10 ± 0.59	3.60 ± 0.80
Fine grained (Phu Phan) sandstone	S3-UCS-01	1.0	14.10	0.24	5.69	5.26
	S3-BI-02	0.5	10.07	0.26	4.00	4.33
	S3-BI-03	0.0	11.34	0.28	4.43	5.64
	S3-BI-04	-0.5	11.45	0.25	4.58	4.58
	S3-BI-05	-1.0	10.46	0.29	4.05	5.00
Average ± SD			11.48 ± 1.57	0.26 ± 0.02	4.55 ± 0.68	4.96 ± 0.52
Fine grained (Phra Wihan) sandstone	S4-UCS-01	1.0	13.00	0.26	5.14	5.57
	S4-BI-02	0.5	10.98	0.26	4.36	4.72
	S4-BI-03	0.0	11.91	0.28	4.65	5.92
	S4-BI-04	-0.5	12.17	0.28	4.76	6.05
	S4-BI-05	-1.0	11.21	0.29	4.35	6.00
Average ± SD			11.85 ± 0.81	0.27 ± 0.01	4.65 ± 0.33	5.65 ± 0.55

Table 5.3 Summary of elastic parameters

Rock Name	Specimen No.	Lode parameter (L)	E (MPa)	ν	G (GPa)	λ (GPa)
Siltstone	ST-UCS-01	1.0	10.90	0.23	4.43	3.77
	ST-BI-02	0.5	12.66	0.27	4.98	5.85
	ST-BI-03	0.0	13.95	0.24	5.54	6.00
	ST-BI-04	-0.5	11.19	0.30	4.30	6.46
	ST-BI-05	-1.0	10.30	0.24	4.14	3.82
Average ± SD			11.80 ± 1.48	0.26 ± 0.03	4.68 ± 0.58	5.18 ± 1.28

CHAPTER VI

STRENGTH CRITERIA

6.1   Introduction

This chapter describes strength criteria for describing results of uniaxial and biaxial compression tests. They include Hoek-Brown, Mogi, and modified Wiebols and Cook criteria. The mean misfit is determined for each criterion and is used as an indicator of its performance. Analytical solution is applied to demonstrate effect of σ_2 on the factor of safety (FS) for stability analysis of a circular tunnel.

6.2   Lode parameter

Lode (1926) tests tubes of steel, copper, and nickel under various combinations of longitudinal tension and internal hydrostatics pressure. Lode derives a sensitive method of differentiating the effect of intermediate principal stress on yielding. For this study, Lode parameter (L) defines the effect of σ_2 on strength of rock specimens. This parameter has values ranging from -1 to $+1$. The parameter equals to 1 for uniaxial compression, -1 for biaxial compression and between -1 to 1 for polyaxial compression. It can be calculated as:

$$L = (2\sigma_2 - \sigma_3 - \sigma_1) / (\sigma_3 - \sigma_1) \tag{6.1}$$

where $\sigma_1, \sigma_2,$ and σ_3 are major, intermediate and minor principal stresses.

6.3   Predictability of strength criteria

Strength criteria are used to compare against the strength data in the form of major principal stress at failure as a function of intermediate principal stress. The predictive capability of each strength criterion is determined using mean misfit as an indicator. The mean misfit ($\bar{s}$) for each criterion can be calculated by Riley et al.,

(1998) as:

$$\bar{s} = \frac{1}{m}\sum_i s_i = \sqrt{\frac{1}{n}\sum_{j=1}^{n}(\sigma_{1,j}^{calc} - \sigma_{1,j}^{test})^2} \qquad (6.2)$$

where $\sigma_{1,j}^{calc}$ is the maximum stress predicted from strength criterion, $\sigma_{1,j}^{test}$ is the maximum stress from measured strengths, n is number of intermediate principal stress or data points, and m is number of data sets. The lower misfit value indicates good predictability.

6.4   Hoek and Brown criterion

Hoek and Brown criterion in the form of J_2 (second-order invariant of stress) and $\sigma_{m,2}$ can be expressed as (Hoek and Brown, 1980):

$$J_2^{1/2} = \frac{2}{\sqrt{3}}(\sigma_{m,2}) \qquad (6.3)$$

where $\sigma_{m,2} = (\sigma_1 + \sigma_3)/2$ \qquad (6.4)

by $J_2^{1/2} = [1/6((\sigma_1 - \sigma_2)^2 + (\sigma_1 - \sigma_3)^2 + (\sigma_2 - \sigma_3)^2)$ \qquad (6.5)

The Hoek and Brown criterion defines the relationship between the maximum and minimum stresses (Hoek and Brown, 1980) by:

$$\sigma_1 = \sigma_3 + \sigma_c\sqrt{m'\frac{\sigma_3}{\sigma_c} + s} \qquad (6.6)$$

where m and s are constants that depend on the properties of rocks and on the extent to which it had been before being subjected to the failure stresses σ_1 and σ_3. Table 6.1 shows calibrated parameters of Hoek and Brown criterion with mean misfit

values. Figure 6.1 compares the prediction of Hoek and Brown criterion with test results. It tends to overestimate the rock strengths, particularly under high σ_2 values.

Table 6.1   Parameters of Hoek and Brown criterion with mean misfit values

Rock Type	σ_c (MPa)	s	m (MPa^{-1})	Mean Misfit (MPa)
Granite	55.0	1.0	65.4	10.36
Limestone	44.4	1.0	18.9	6.36
Marble	28.2	1.0	10.0	6.65
Gypsum	9.3	1.0	6.2	2.69
Coarse grained sandstone	34.4	1.0	15.7	16.57
Medium grained sandstone	28.3	1.0	12.7	5.93
Fine grained sandstone	36.4	1.0	14.9	21.55
Fine grained (Phra Wihan) sandstone	30.3	1.0	22.7	22.68
Siltstone	27.7	1.0	19.0	15.70
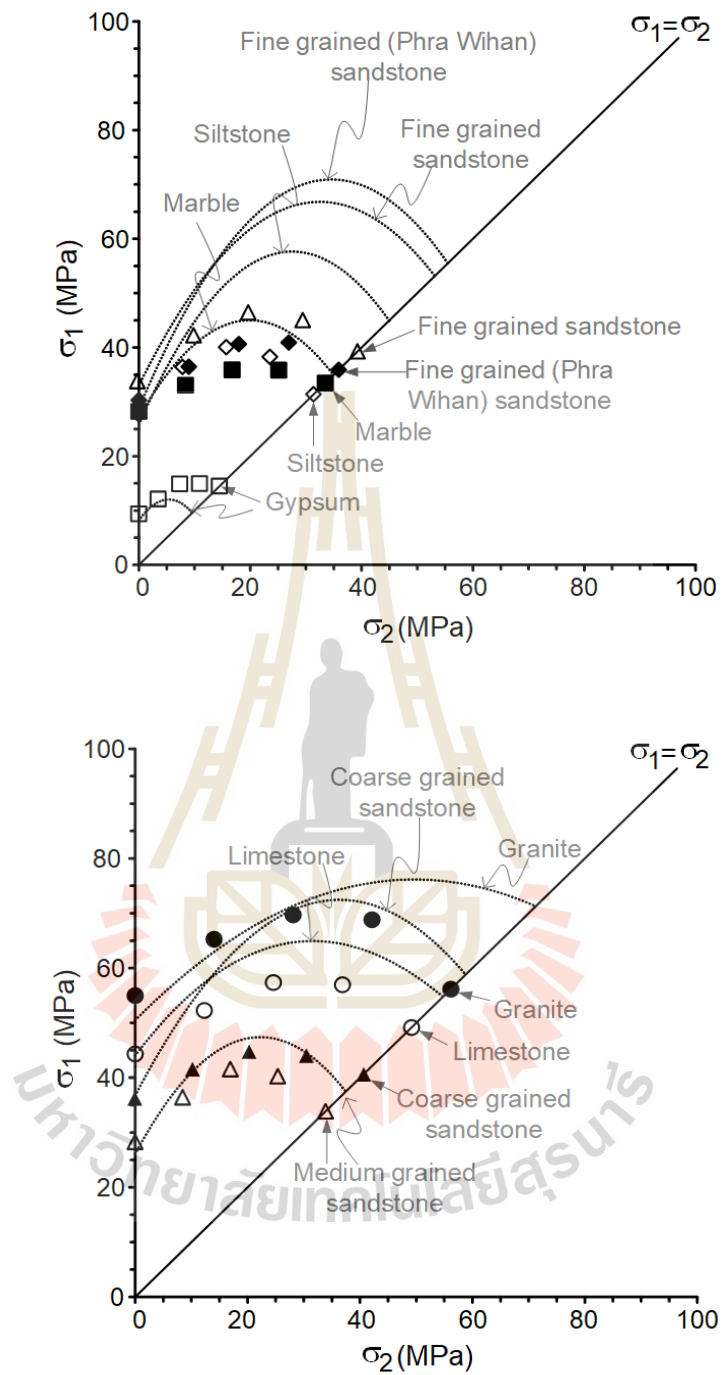
Figure 6.1 Hoek and Brown criterion (line)

as compared to test results (points)

6.5   Mogi criterion

The mogi (1971) is a generalization form of the von Mises's theory. It is formulated by (Mogi, 1967):

$$\tau_{oct} = f_1(\sigma_{m,2}) \tag{6.7}$$

where f_1 is a monotonically increasing function. τ_{oct} and $\sigma_{m,2}$ are octahedral shear stress and effective mean stress, respectively. The empirical Mogi criterion uses a power law to describe the failure stresses, and defines τ_{oct} at failure in terms of $\sigma_{m,2}$ as:

$$\tau_{oct} = A' \, \sigma_{m,2}^{B'} \tag{6.8}$$

$$\tau_{oct} = \sqrt{\left(\frac{1}{3}\right)\{(\sigma_1 - \sigma_2)^2 + (\sigma_1 - \sigma_3)^2 + (\sigma_2 - \sigma_3)^2\}} \tag{6.9}$$

$$\sigma_{m,2} = \frac{(\sigma_1 + \sigma_2)}{2} \tag{6.10}$$

Constants A' and B' depend on rock materials, as shown in Table 6.2. Figure 6.2 compares Mogi criterion with test results. The empirical (power law) Mogi criterion slightly overestimates the rock strengths, particularly under high σ_2 values.

Table 6.2   Parameters of Mogi criterion with mean misfit values

Rock Type	A'	B'	Mean Misfit (MPa)
Granite	7.174	0.390	5.65
Limestone	6.116	0.403	2.34
Marble	3.785	0.479	2.26
Gypsum	1.205	0.829	2.44
Coarse grained sandstone	4.262	0.477	3.57
Medium grained sandstone	2.807	0.596	4.18
Fine grained sandstone	7.460	0.293	2.83
Fine grained (Phra Wihan) sandstone	3.502	0.523	1.29
Siltstone	2.947	0.574	9.70
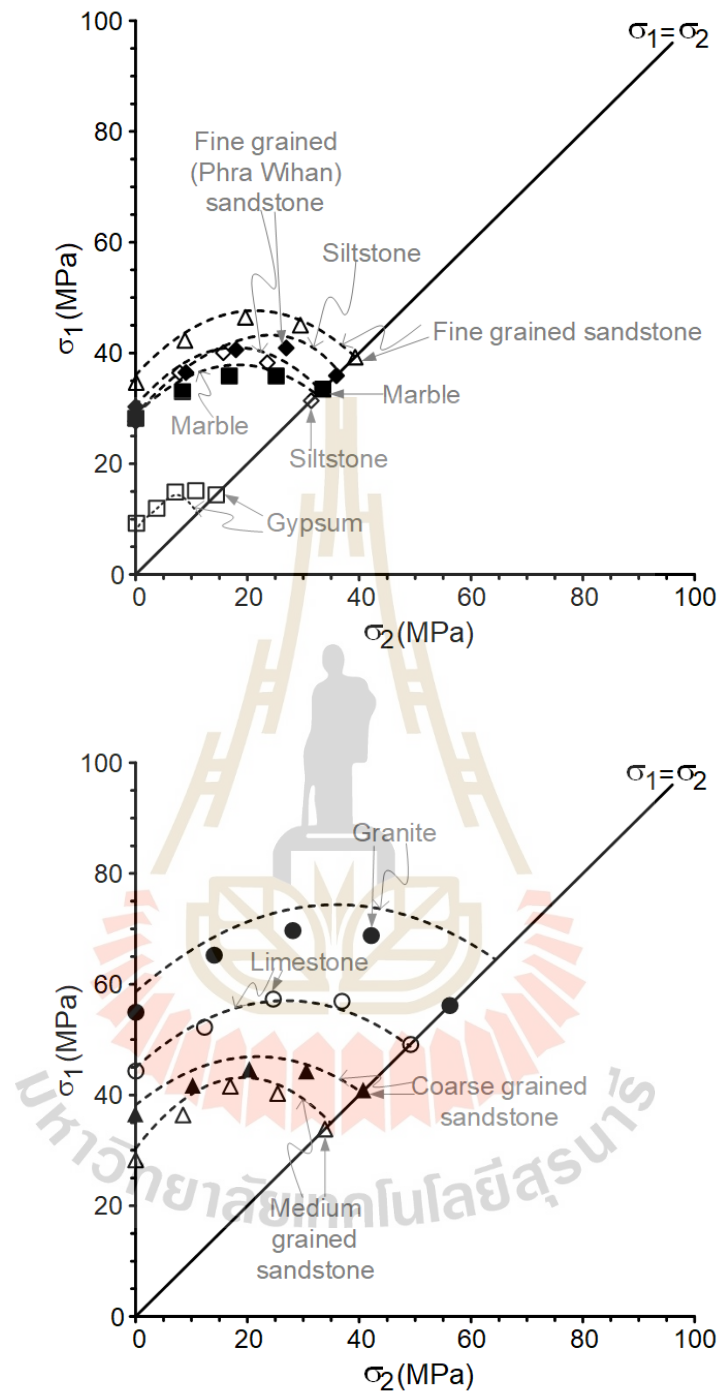
Figure 6.2 Mogi criterion (dash line)

as compared to test results (points)

6.6 Modified Wiebols and Cook criterion

Modified Wiebols and Cook criterion is used to describe the test results as it is capable of incorporating all three principal stresses at failure. This multi-axial strength criterion has been used by several investigations (Cai, 2008; Komenthammasopon and Fuenkajorn, 2015; Chang and Haimson, 2000; Mehranpour and Kulatilake, 2016; Zhang et al., 2017; Artkhonghan et al., 2018) in particular to assess the effect of intermediate principal stress (σ_2) on failure stress (σ_1) under various confining pressures. The criterion is proposed by Zhou (1994) as originally developed by Wiebols and Cook (1968). It is based on the increase in energy around the Griffith crack due to the sliding of crack surfaces over each other. The modified version defined $J_2^{1/2}$ (second-order invariant of stress) at failure in terms of J_1 (first-order invariant of stress) or σ_m (mean stress) as:

$$J_2^{1/2} = A + BJ_1 + CJ_1^2 \tag{6.11}$$

by $J_1 = \sigma_m = (1/3)(\sigma_1 + \sigma_2 + \sigma_3)$. The constants A, B, and C depend on internal friction angle (ϕ) and uniaxial compressive strength (σ_c). They can be calculated as follows:

$$A = \sigma_c/\sqrt{3} - B\sigma_c/3 - C\sigma_c^2/9 \tag{6.12}$$

$$B = \sqrt{3}(q-1)/(q+2) - C/3(2\sigma_c + (q+2)\sigma_3) \tag{6.13}$$

$$C = [\sqrt{27}/(2C_1 + (q-1)\sigma_3 - \sigma_c)] \{[(C_1 + (q-1)\sigma_3 - \sigma_c)/$$
$$(2C_1 + (2q+1)\sigma_3 - \sigma_c)] - [(q-1)/(q+2)]\} \tag{6.14}$$

where q can be calculated from a coefficient of internal friction (μ) of the material or internal friction angle (ϕ) depending on the properties of the rock, $\mu = \tan\phi$, $q = [(\mu^2+1)^{1/2} + \mu]^2 = \tan^2(\pi/4 + \phi/2)$, and $C_1 = (1+0.6\mu)\sigma_c$. Substitute all variables into equations (6.11), through (6.13), the $J_2^{1/2}$ at failure can be calculated for each rock

type. Constants A, B, and C are shown in Table 6.3. From the test results $J_2^{1/2}$ can be calculated by Jaeger et al., (2007):

$$J_2^{1/2} = [1/6((\sigma_1-\sigma_2)^2+(\sigma_1-\sigma_3)^2+(\sigma_2-\sigma_3)^2) \qquad (6.15)$$

Figure 6.3 compares the prediction failure envelopes with the test results. The predictive capability of the proposed strength criterion for the nine tested rocks is determined using the mean misfit as an indicator. The lower misfit value indicates good predictability and are shown in Table 6.3, suggesting that the Wiebols and Cook criterion fits well to rock strengths under biaxial conditions.
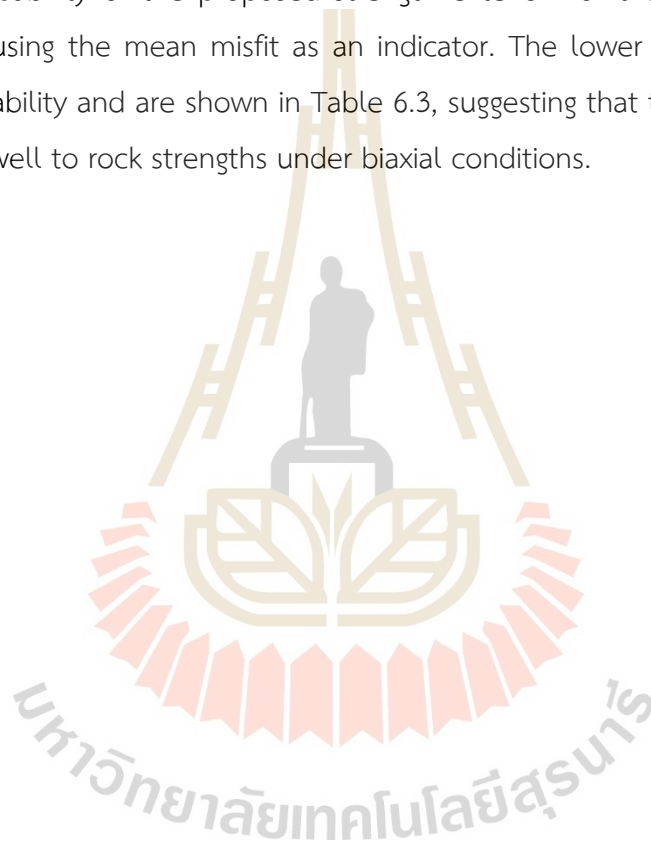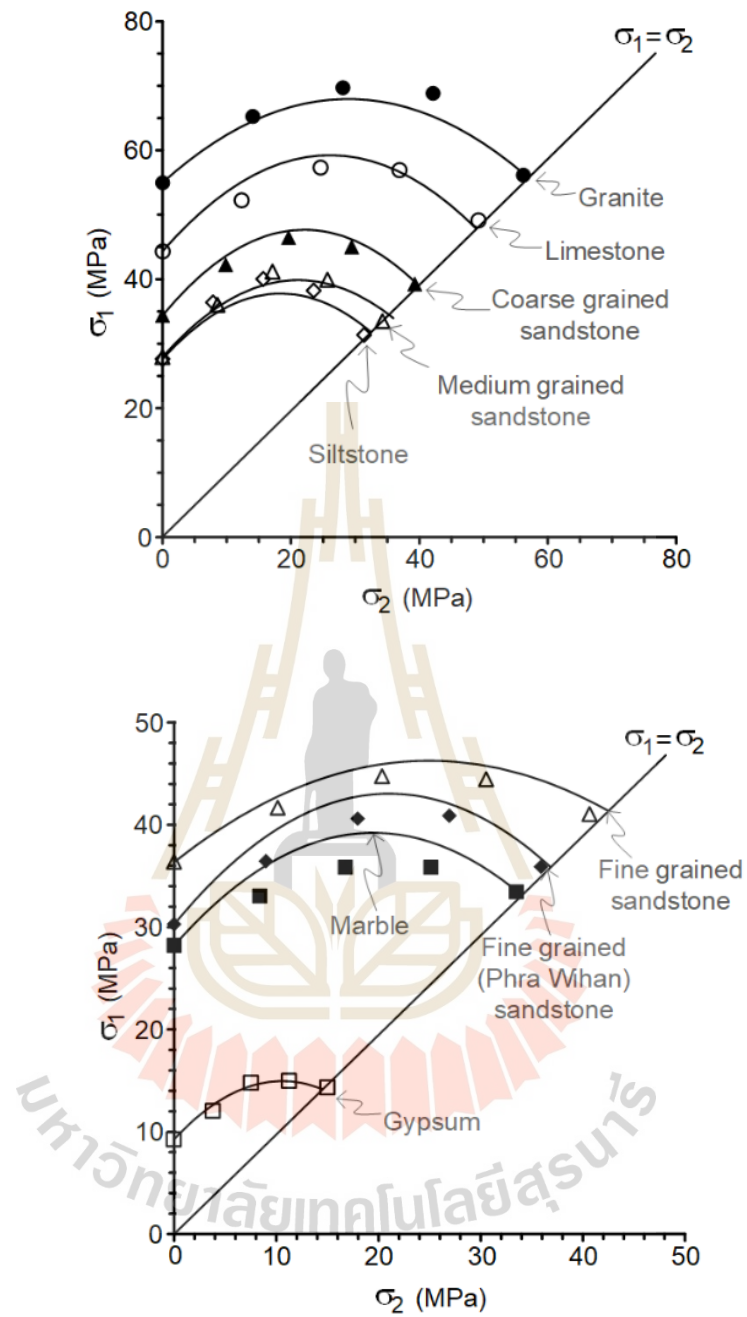
Figure 6.3 Modified Wiebols and Cook criterion (line)

as compared to test results (points)

Table 6.3 Parameters of modified Wiebols and Cook criterion with mean
misfit values

Rock Type	A (MPa)	B	C (MPa^{-1})	$J_2^{1/2}$ (MPa)	ϕ (degrees)	Mean Misfit (MPa)
Granite	54.983	0.899	-0.016	33.66	60.0	1.82
Limestone	44.363	1.161	-0.023	27.80	48.0	1.92
Marble	28.223	1.130	-0.029	17.83	37.0	1.60
Gypsum	9.276	1.133	-0.055	7.04	23.0	0.33
Coarse grained sandstone	34.398	1.204	-0.027	22.17	44.0	0.92
Medium grained sandstone	28.273	1.148	-0.028	19.24	40.0	1.14
Fine grained sandstone	36.348	0.846	-0.018	22.19	44.0	1.20
Fine grained (Phra Wihan) sandstone	30.298	1.239	-0.030	19.67	47.0	0.74
Siltstone	27.657	1.139	-0.032	18.55	45.0	1.52

Under biaxial compressive stresses the modified Wiebols and Cook criterion can predict the compressive strengths of all tested rocks reasonably well. This agrees with the results obtained by Haimson (2000) and Colmenares and Zoback (2002). Due to the effect of σ_2 Hoek and Brown criterion cannot represent rock strengths under biaxial compression condition, particularly under high σ_2 and has discrepancy larger than Mogi, as indicated by the mean misfit values.

6.7   Analysis of test results

Stress around a circular hole in an infinite plate is proposed to demonstrate the effect of σ_2 on the stability of a tunnel. This assumes that rock surrounding the cylindrical tunnel behaves as a linearly elastic material. The equation for solving this

problem is widely used and is commonly referred to as Kirsch solution (Jaeger et al., 2007). The equation assumes that the tunnel is under plane strain condition. At tunnel boundary, the stress states can be obtained as:

$$\sigma_\theta = 2P_0, \tag{6.16}$$

$$\sigma_r = 0 \tag{6.17}$$

where σ_θ is tangential stress, P_0 is uniform external stress, and σ_r is radial stress. The axial stress (σ_z) along the tunnel axis can be calculated as:

$$\sigma_z = [\nu/(1-\nu)]\sigma_\theta \tag{6.18}$$

where ν is the Poisson's ratio of rock. At the opening boundary the factor of safety (FS) can be obtained as:

$$FS = \sigma_{Wiebols}/\sigma_\theta \tag{6.19}$$

where $\sigma_{Wiebols}$ is the rock strengths according to the modified Wiebols and Cook criterion. Figure 6.4 plots the factor of safety on the circular opening boundary, comparing the conventional approach (σ_c/σ_θ) with those considered the effect of σ_2 ($\sigma_{Wiebols}/\sigma_\theta$). The diagram demonstrates that FS from $\sigma_{Wiebols}/\sigma_\theta$ has a greater safety value than σ_c/σ_θ. The two approaches are identical only when L = 1.0 or ν = 0 (no σ_2 effect). The factor of safety increases to the maximum when L decreases toward 0 or when ν increases to 0.33. This condition represents the maximum effect of the intermediate principal stress. The factor of safety (FS) of the biaxial strength is higher than uniaxial compressive strength. Figure 6.5 shows the magnitudes and directions of tangential, radial and axial stresses at the opening boundary.
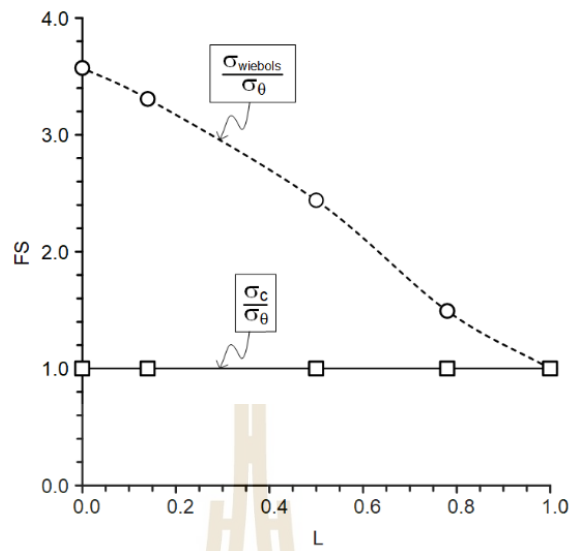
Figure 6.4   Factor of safety (FS) for biaxial strength ($\sigma_{Wiebols}/\sigma_\theta$) and uniaxial strength (σ_c/σ_θ) as a function of Lode parameters
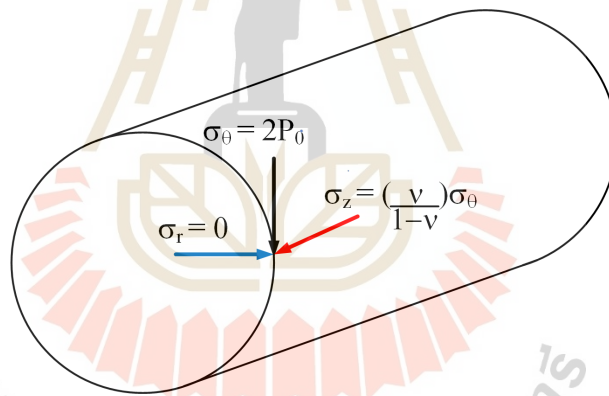
Figure 6.5 Stresses at opening boundary under plane strain condition

CHAPTER VII

DISCUSSIONS AND CONCLUSIONS

7.1 Discussions

This study determines the effects of intermediate principal stress on rock strength by biaxial test method. The results are compared against strength criteria developed by Hoek and Brown (1980), Mogi (1971), and modified Wiebols and Cook (1968).

Lode parameters are used to describe stress state conditions depending on σ_1. The strength results clearly show that σ_2 affects the maximum stress σ_1, at failure for all tested rocks. The effect of σ_2 on rock strength is prominent as explicitly shown by test results.

Multiple extensile fractures occur at L=0 or less due to the fracture initiation has influence from the σ_2 direction. This results in a lower σ_1 at failure. When σ_2 is lower or L>0, only σ_1 contributes to shear fracture initiation. This results in a higher σ_1 at failure as compared to the curves where L≤0. The failure mode of biaxial test show multiple extensile fractures parallel to σ_1-σ_2 plane cause rock split toward free surface, particularly for strong rocks which agree with those of other researchers (Sahouryeh et al., 2002; Zhu et al., 2005; Cai, 2008; Garg et al., 2018). Due to the failure mechanisms described above the highest rock strength (σ_1 at failure) tends to occur under L=0.

Under biaxial compression, modified Wiebols and Cook can predict the rock strengths reasonably well. Hoek and Brown criterion and Mogi cannot represent the rock strengths under biaxial compression because they exclude σ_2 from the equations, they have overestimated the test results. This is in agreement with result to obtained by Yun et al. (2010) and Haimson and Rudnicki (2010) that Hoek and Brown criterion disregards the effect of σ_2, it is a poor correlation for biaxial loading. Therefore, they may not a suitable for analyzing rocks under biaxial conditions.

For the calculation of the factor of safety (FS) of circular opening boundary presented here, it suggests that the factor of safety calculation from modified Wiebols and Cook is not too conservative and is more appropriate than the analysis of FS from uniaxial strength.

7.2 Conclusions

All objectives and requirements of this study have been met. The results of the laboratory testing and analyses can be summarized as follows:

1) Elastic parameters (E) and Poisson's ratio (ν) tend to be independent of the Lode parameter. Some variation of E and ν may be due to the intrinsic variability of the rocks.

2) For uniaxial test, stress-strain curve has dilation of ε_2 and ε_3 with similar expansion values. For biaxial test, the lateral strains extend differently due to σ_2 effect resulting in less dilatation of ε_2 than ε_3 which is subjected to free surface as minimum stress (σ_3) equal zero.

3) Under low σ_2, fracture appearance of rock specimens show compressive shear failures. While under higher σ_2, rock specimens show multiple extensile fractures parallel to σ_1- σ_2 plane, particularly for strong rocks.

4) Intermediate principal stress (σ_2) affects rock strength. The strengths initially increase with increasing σ_2 or with decreasing Lode parameters (L). The failure stresses are reached at the Lode parameter of about -0.5. Below and above L = -0.5, the major principal stress at failure decreases.

5) The modified Wiebols and Cook criterion can describe the rock strengths under biaxial conditions with low mean misfit value of all tested rock.

6) Factor of safety (FS) of circular opening in infinite plate analyzed from biaxial strengths are always higher than those from uniaxial compressive strength. When L = 1.0 or ν = 0, there is no σ_2 effect. The factor of safety increases to the maximum when L decreases toward 0 or when ν increases to 0.33. This condition represents the maximum effect of the intermediate principal stress.

7.3   Recommendations for future studies

More testing is recommended to assess the effect of the intermediate principal stress on rock strength under biaxial stress state.

1)   Studying of σ_2 effect on a variety of rocks with a broad range of strengths should be performed to show fracture characteristics, particularly in soft rocks. Since fractures are more pronounced in strong rocks, such as granite, limestone, marble, and sandstone. The fracture characteristics of soft rocks, such as gypsum may be caused by other mechanisms, such as grain sizes, porosity, fissures, microcracks or types of rock-forming minerals.

2)   The effects of loading rate and time-dependency should be considered under biaxial stresses. It is well known that high loading rates lead to higher rock strength but when the intermediate principal stress is involved, the evolution of rock strength remains unclear. By considering the effects of loading rate and time-dependency, the biaxial stress analysis can provide a more understanding of how the rock strength changes under in-situ condition.

3)   The effect of temperature should be considered on biaxial compression test. The specimens should be tested under a broad range of temperatures in relation to depth. Opening at great depth, temperature variations can induce thermal stress in a surrounding rock.

REFERENCES

Alsayed, M. I. (2002). Utilising the Hoek triaxial cell for multiaxial testing of hollow rock cylinders. *International Journal of Rock Mechanics and Mining Sciences. 39*(3), 355-366.

Arora, S. and Mishra, B. (2015). Investigation of the failure mode of shale rocks in biaxial and triaxial compression tests. *International Journal of Rock Mechanics and Mining Sciences, 79*, 109-123.

Artkhonghan, K., Sartkaew, S., Thongprapha, T., and Fuenkajorn, K. (2018). Effects of stress path on shear strength of a rock salt. *International Journal of Rock Mechanics and Mining Sciences, 104*, 78-83.

ASTM D7012-14. (2014). *Standard Test Methods for Compressive Strength and Elastic Moduli of Intact Rock Core Specimens under Varying States of Stress and Temperatures.* Annual Book of ASTM Standards, West Conshohocken, Pennsylvania, USA.

ASTM D7263-09. (2018). *Standard Test Methods for Laboratory Determination of Density (Unit Weight) of Soil Specimen*. Annual Book of ASTM Standards, West Conshohocken, Pennsylvania, USA.

Brady, B.H.G. and Brown, E.T. (2006). Rock Mechanics for Underground Mining, 3rd ed. Dordrecht, Netherlands: Springer.

Cai, M. (2008). Influence of intermediate principal stress on rock fracturing and strength near excavation boundaries-insight from numerical modeling. *International Journal of Rock Mechanics and Mining Sciences, 45*(5), 763-772.

Chang, C., and Haimson, B. (2000). True triaxial strength and deformability of the German Continental Deep Drilling Program (KTB) deep hole amphibolite. *Journal of Geophysical Research: Solid Earth, 105*(B8), 18999-19013.

Colmenares, L. B. and Zoback, M. D. (2002). A statistical evaluation of intact rock failure criteria constrained by polyaxial test data for five different rocks. *International Journal of Rock Mechanics and Mining Sciences, 39*(6), 695-729.

Fakhimi, A., Carvalho, F., Ishida, T., and Labuz, J. F. (2002). Simulation of failure around a circular opening in rock. *International Journal of Rock Mechanics and Mining Sciences, 39*(4), 507-515.

Fuenkajorn, K., Sriapai, T., and Samsri, P. (2012). Effects of loading rate on strength and deformability of Maha Sarakham salt. *Engineering Geology, 135*, 10-23.

Garg, P., Pandit, B., and Mishra, B. (2018). *Investigation of the failure mode of intact rock in biaxial compression tests.* In 52nd US Rock Mechanics/Geomechanics Symposium. American Rock Mechanics Association. West Virginia University, USA. 18– 1278.

Haimson, B. (2006). True triaxial stresses and the brittle fracture of rock. *Pure and Applied Geophysics, 163*, 1101-1130.

Haimson, B. and Rudnicki, J. W. (2010). The effect of the intermediate principal stress on fault formation and fault angle in siltstone. *Journal of Structural Geology, 32*(11), 1701-1711.

Handin, J., Heard, H. A., and Magouirk, J. N. (1967). Effects of the intermediate principal stress on the failure of limestone, dolomite, and glass at different temperatures and strain rates. *Journal of geophysical research, 72*(2), 611-640.

Jaeger, J.C., Cook, N. G. W., and Zimmerman, R. W. (2007). Fundamentals of Rock Mechanics, 4th ed. Blackwell, *Maiden, MA*.

Khamrat, S., Archeeploha, S., and Fuenkajorn, K. (2016). Pore pressure effects on strength and elasticity of ornamental stones. *Scienceasia, 42*, 121-135.

Komenthammasopon, S., and Fuenkajorn, K. (2015). Effects of stress path on biaxial strengths of sandstones. *Engineering Journal of Research and Development, 26*(2), 49-57.

Liu, K., Zhao, J., Wu, G., Maksimenko, A., Haque, A., and Zhang, Q. B. (2020). Dynamic strength and failure modes of sandstone under biaxial compression. *International Journal of Rock Mechanics and Mining Sciences, 128*, 104260.

Lode, W. (1926). Versuche über den Einfluß der mittleren Hauptspannung auf das Fließen der Metalle Eisen, Kupfer und Nickel. *Zeitschrift für Physik, 36*(11-12), 913-939.

Mehranpour, M. H., and Kulatilake, P. H. (2016). Comparison of six major intact rock failure criteria using a particle flow approach under true-triaxial stress condition. *Geomechanics and geophysics for geo-energy and geo-resources, 2*, 203-229.

Mogi, K. (1967). Effect of the intermediate principal stress on rock failure. *Journal of Geophysical Research, 72*(20), 5117-5131.

Mogi, K. (1971). Fracture and flow of rocks under high triaxial compression. *Journal of Geophysical Research, 76*(5), 1255-1269.

Murrell, S.A.F. (1963). A criterion for brittle fracture of rocks and concrete under triaxial stress and the effect of pore pressure on the criterion. *Rock mechanics*, 563-577.

Rao, K.S. and Tiwari, R.P. (2002). Physical simulation of jointed model materials under biaxial and true triaxial stress states. *Research Report, IIT Delhi, India,* 30.

Riley, K.F., Hobson, M.P., and Bence, S.J. (1998). Mathematical Methods for Physics and Engineering. *A Comprehensive Guide. [Quantum operators]*, 648-712.

Sahouryeh, E., Dyskin, A. V., and Germanovich, L. N. (2002). Crack growth under biaxial compression. *Engineering Fracture Mechanics, 69*(18), 2187-2198.

Sagong, M., Park, D., Yoo, J., and Lee, J. S. (2011). Experimental and numerical analyses of an opening in a jointed rock mass under biaxial compression. *International Journal of Rock Mechanics and Mining Sciences, 48*(7), 1055-1067.

Sriapai, T., Walsri, C., and Fuenkajorn, K. (2013). True-triaxial compressive strength of Maha Sarakham salt. *International Journal of Rock Mechanics and Mining Sciences, 61,* 256-265.

Tang, C.A., and Hudson, J.A. (2002). *Understanding rock failure through numerical simulations and implications for the use of codes in practical rock engineering.* In Proceedings of the 5th North American Rock Mechanics Symposium and the 17th Tunnelling Association of Canada Conference. Toronto, Canada. 705-712.

Tiwari, R. P., and Rao, K.S. (2004). Physical modeling of a rock mass under a true triaxial stress state. *International Journal of Rock Mechanics and Mining Sciences, 41*(3), 1-6.

Wiebols, G. A., and Cook, N. G. W. (1968). An energy criterion for the strength of rock in polyaxial compression. *International Journal of Rock Mechanics and Mining Sciences & Geomechanics Abstracts, 5*(6), 529-549.

Yun, X., Mitri, H.S., Yang, X., and Wang, Y. (2010). Experimental investigation into biaxial compressive strength of granite. *International Journal of Rock Mechanics and Mining Sciences, 47*(2), 334-341.

Zhang, H., Wan, Z., Ma, D., Zhang, Y., Cheng, J., and Zhang, Q. (2017). Experimental investigation on the strength and failure behavior of coal and synthetic materials under plane-strain biaxial compression. *Energies, 10*(4), 500.

Zhang, H., Wan, Z., Wang, C., Ma, Z., Zhang, Y., and Cheng, J. (2017). A statistical damage constitutive model for geomaterials under plane-strain biaxial stress state. *Advances in Mathematical Physics, 2017*, 1-10.

Zhu, W.C., and Tang, C.A. (2004). Micromechanical model for simulating the fracture process of rock. *Rock Mechanics and Rock Engineering, 37*, 25–56.

Zhu, W. C., Liu, J. S., Tang, C. A., Zhao, X. D., and Brady, B. H. (2005). Simulation of progressive fracturing processes around underground excavations under biaxial compression. *Tunnelling and Underground Space Technology, 20*(3), 231-247.

APPENDIX A

STRESS-STRAIN CURVES
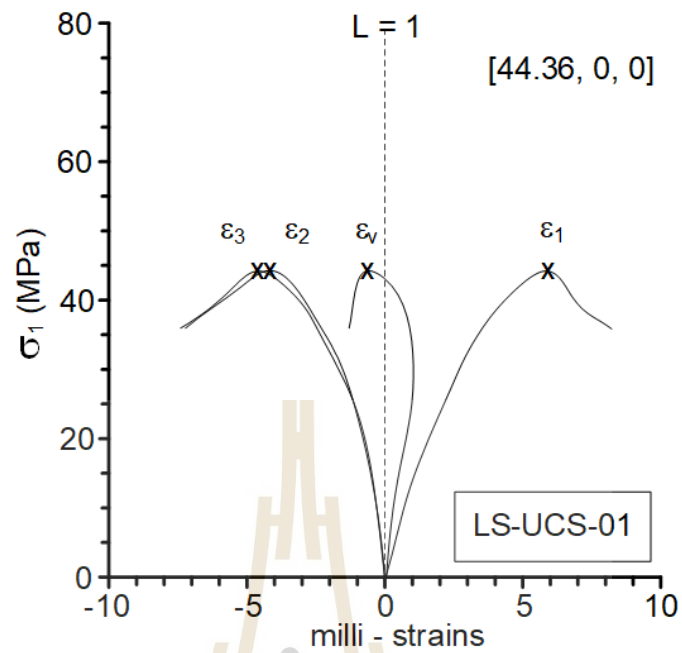
Figure A.1   Stress-strain curves of limestone tested under
$\sigma_2 = 0$ MPa and $\sigma_3 = 0$ MPa.
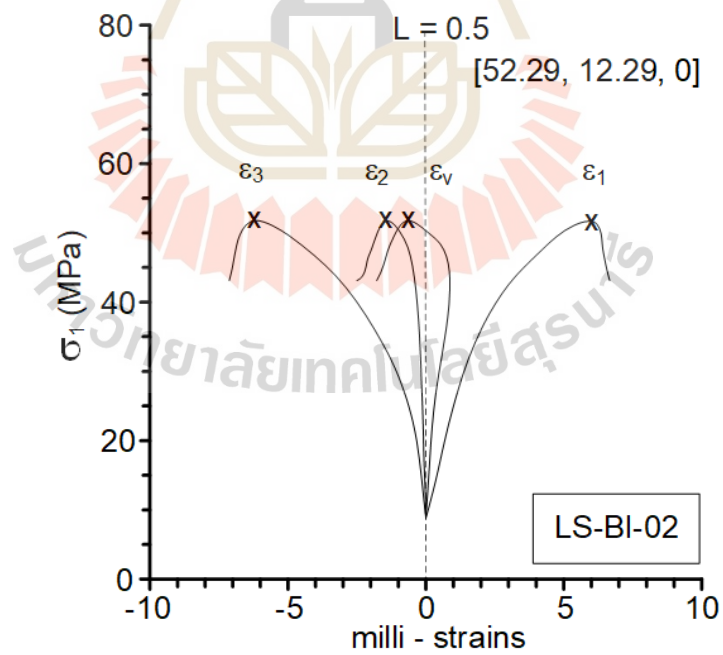
Figure A.2   Stress-strain curves of limestone tested under
$\sigma_2 = 12.29$ MPa and $\sigma_3 = 0$ MPa.
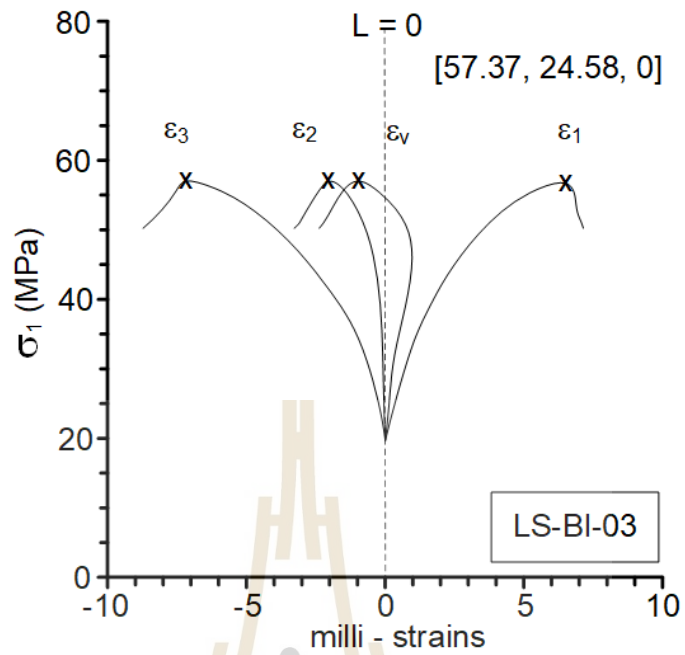
Figure A.3   Stress-strain curves of limestone tested under
σ_2 = 24.58 MPa and σ_3 = 0 MPa.
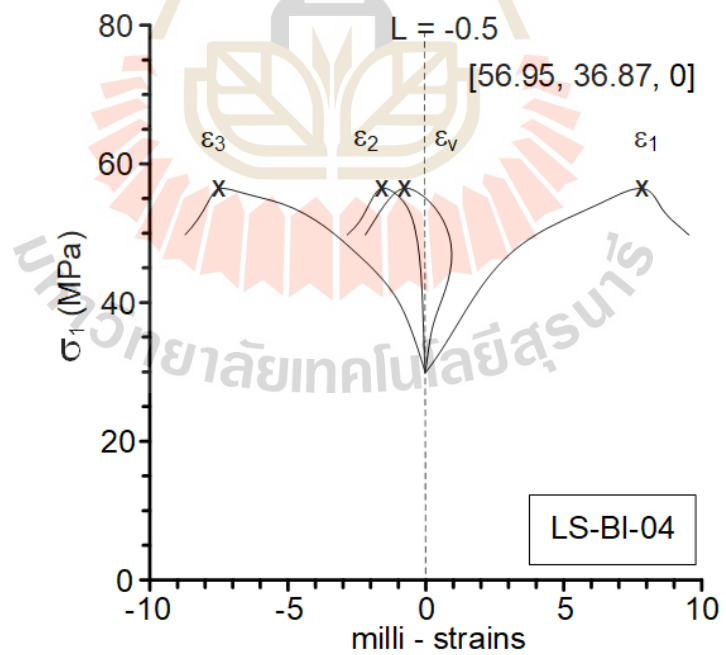
Figure A.4   Stress-strain curves of limestone tested under
σ_2 = 36.87 MPa and σ_3 = 0 MPa.
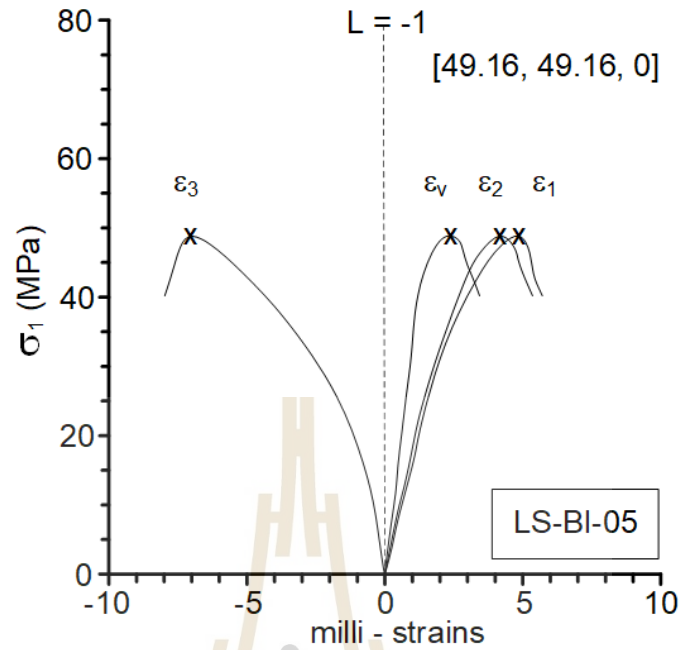
Figure A.5   Stress-strain curves of limestone tested under
σ_2 = 49.16 MPa and σ_3 = 0 MPa.
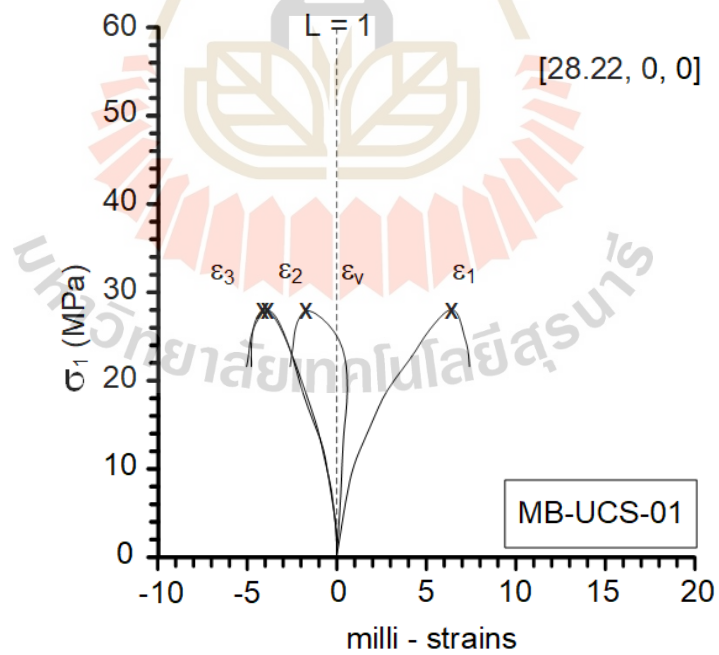
Figure A.6   Stress-strain curves of marble tested under
σ_2 = 0 MPa and σ_3 = 0 MPa.

Figure A.7 Stress-strain curves of marble tested under
σ_2 = 8.37 MPa and σ_3 = 0 MPa.
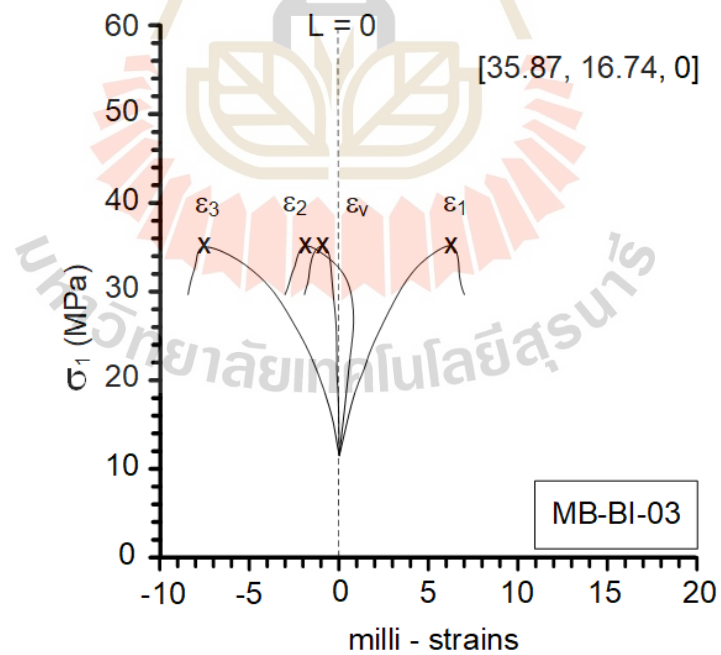
Figure A.8 Stress-strain curves of marble tested under
σ_2 = 16.74 MPa and σ_3 = 0 MPa.
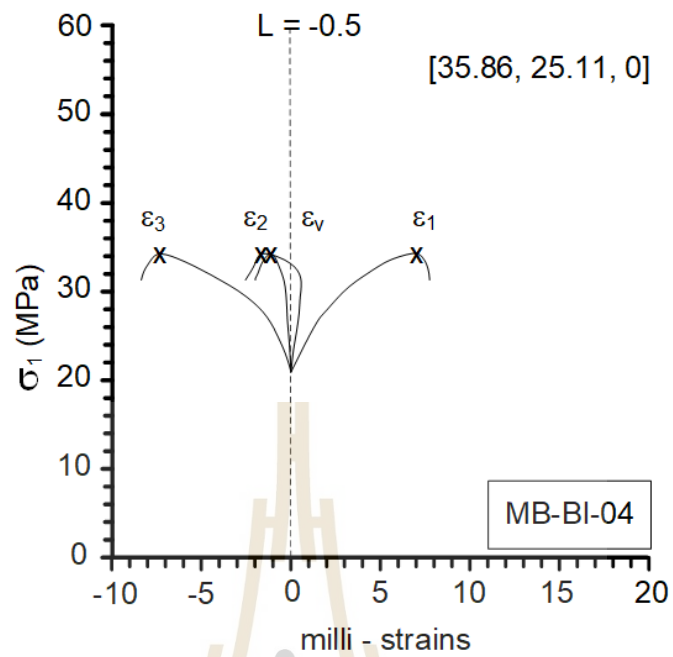
Figure A.9 Stress-strain curves of marble tested under
σ_2 = 25.11 MPa and σ_3 = 0 MPa.
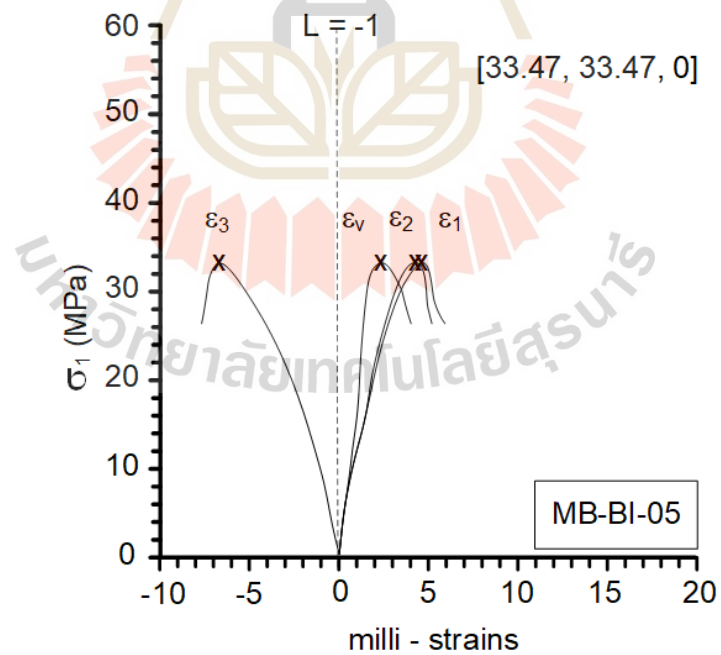
Figure A.10 Stress-strain curves of marble tested under
σ_2 = 33.47 MPa and σ_3 = 0 MPa.
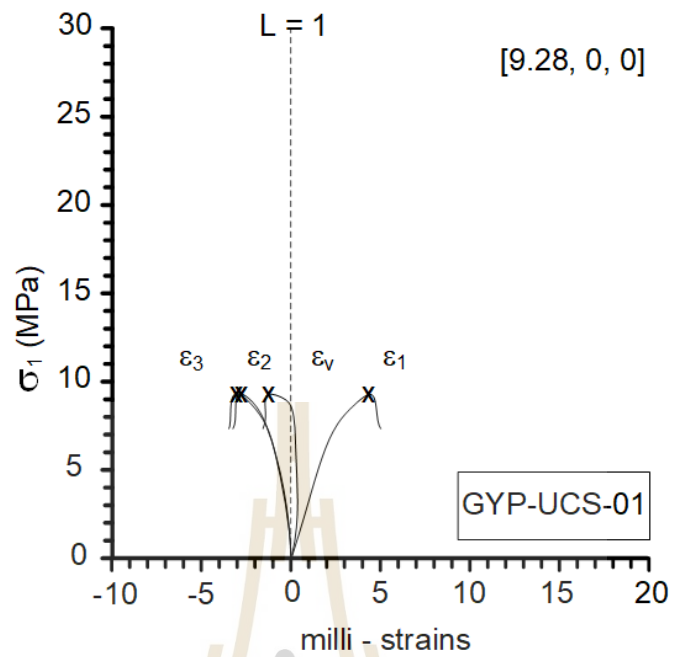
Figure A.11 Stress-strain curves of gypsum tested under
σ_2 = 0 MPa and σ_3 = 0 MPa.

Figure A.12 Stress-strain curves of gypsum tested under
σ_2 = 3.62 MPa and σ_3 = 0 MPa.
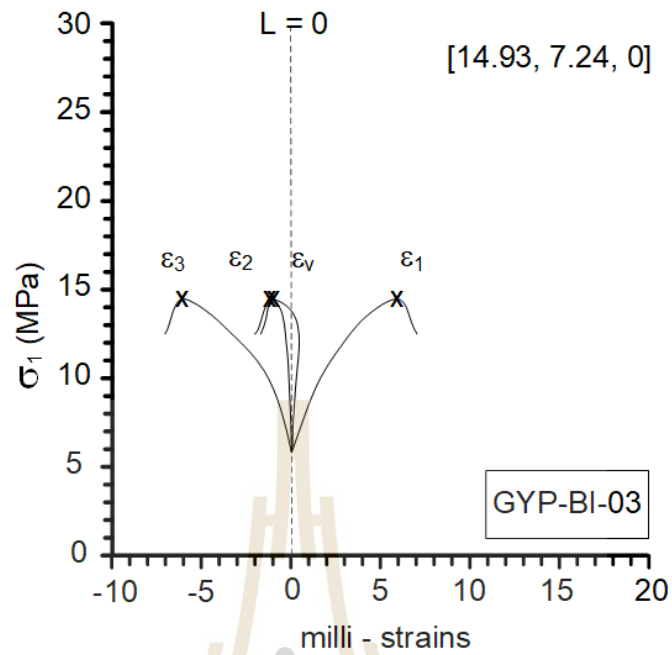
Figure A.13 Stress-strain curves of gypsum tested under
σ_2 = 7.24 MPa and σ_3 = 0 MPa.
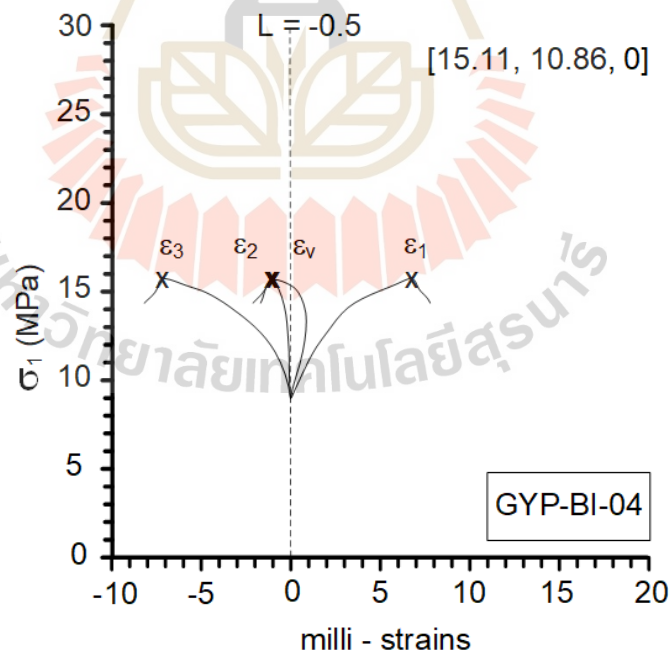
Figure A.14 Stress-strain curves of gypsum tested under
σ_2 = 10.86 MPa and σ_3 = 0 MPa.
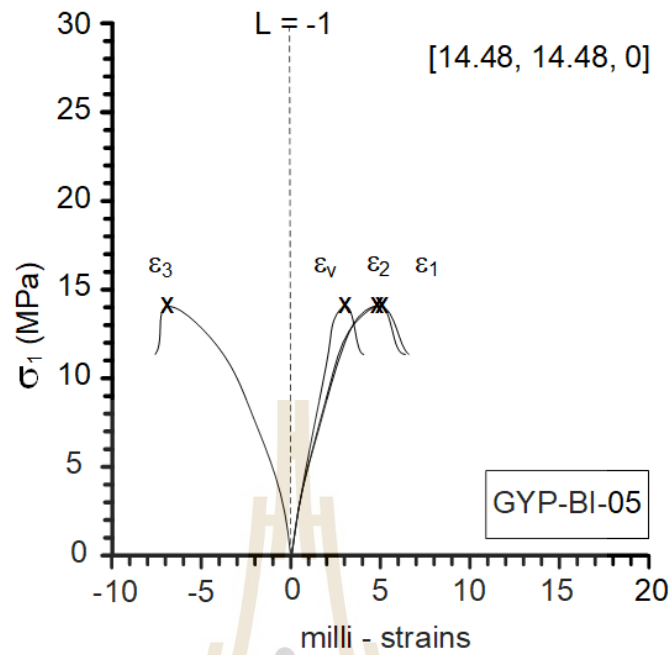
Figure A.15   Stress-strain curves of gypsum tested under
σ_2 = 14.48 MPa and σ_3 = 0 MPa.
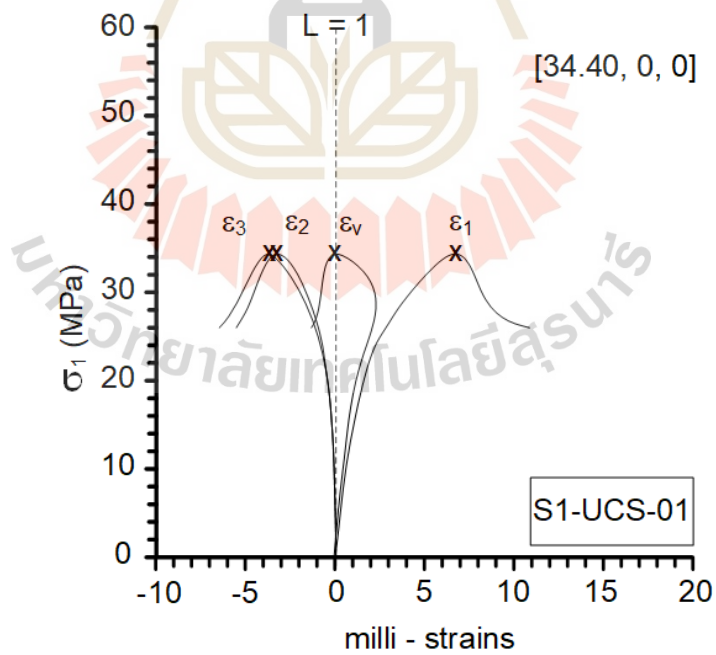
Figure A.16   Stress-strain curves of coarse grained (Phu Phan) sandstone tested under
σ_2 = 0 MPa and σ_3 = 0 MPa.

Figure A.17 Stress-strain curves of coarse grained (Phu Phan) sandstone tested under $\sigma_2 = 9.82$ MPa and $\sigma_3 = 0$ MPa.
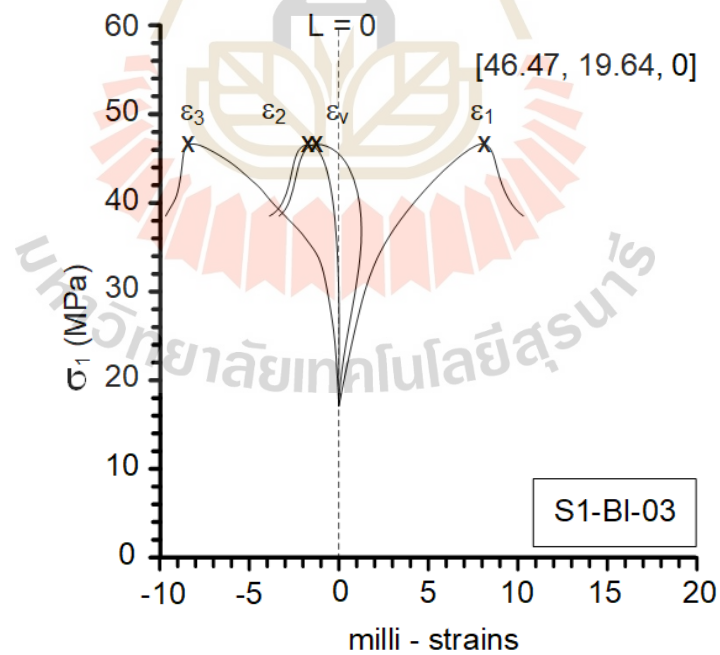
Figure A.18 Stress-strain curves of coarse grained (Phu Phan) sandstone tested under $\sigma_2 = 19.64$ MPa and $\sigma_3 = 0$ MPa.
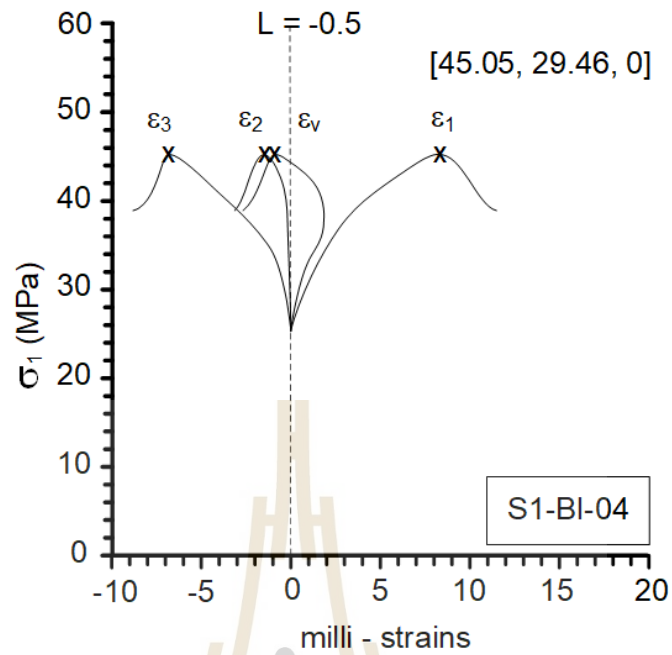
Figure A.19   Stress-strain curves of coarse grained (Phu Phan) sandstone tested under
σ_2 = 29.46 MPa and σ_3 = 0 MPa.
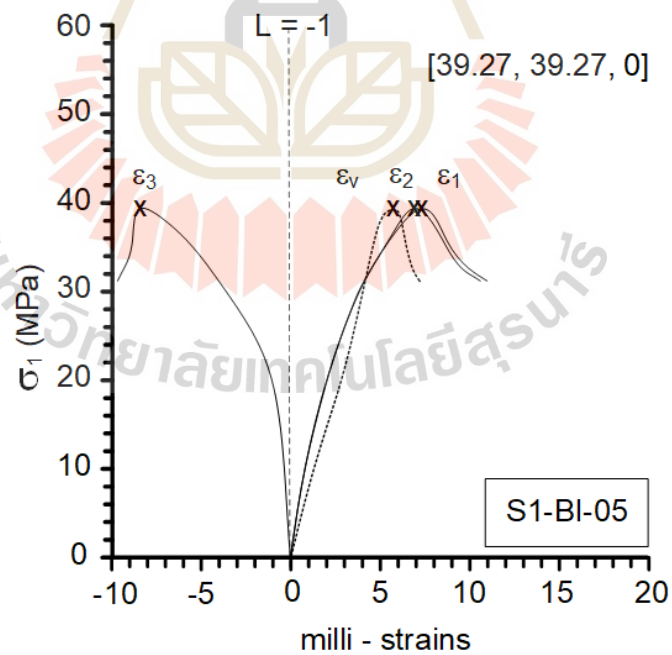
Figure A.20   Stress-strain curves of coarse grained (Phu Phan) sandstone tested under
σ_2 = 39.27 MPa and σ_3 = 0 MPa.
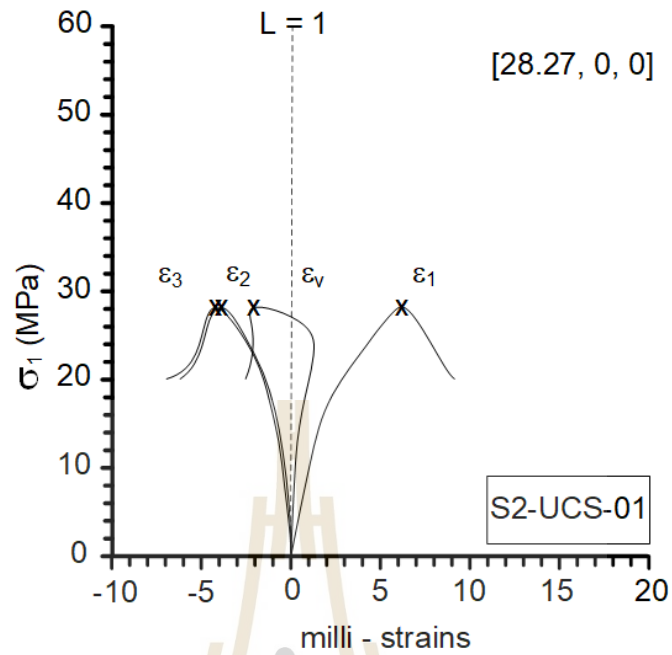
Figure A.21 Stress-strain curves of medium grained (Phu Phan) sandstone tested under σ_2 = 0 MPa and σ_3 = 0 MPa.

Figure A.22 Stress-strain curves of medium grained (Phu Phan) sandstone tested under σ_2 = 8.47 MPa and σ_3 = 0 MPa.
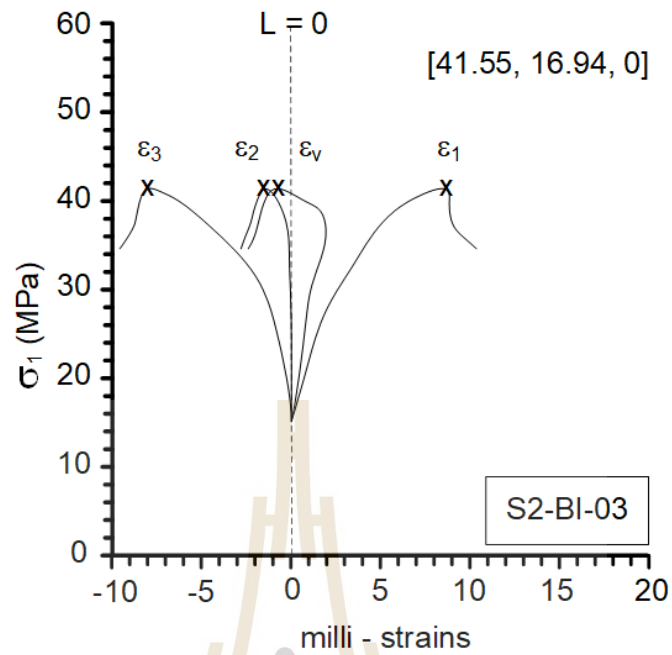
Figure A.23 Stress-strain curves of medium grained (Phu Phan) sandstone tested under σ_2 = 16.94 MPa and σ_3 = 0 MPa.
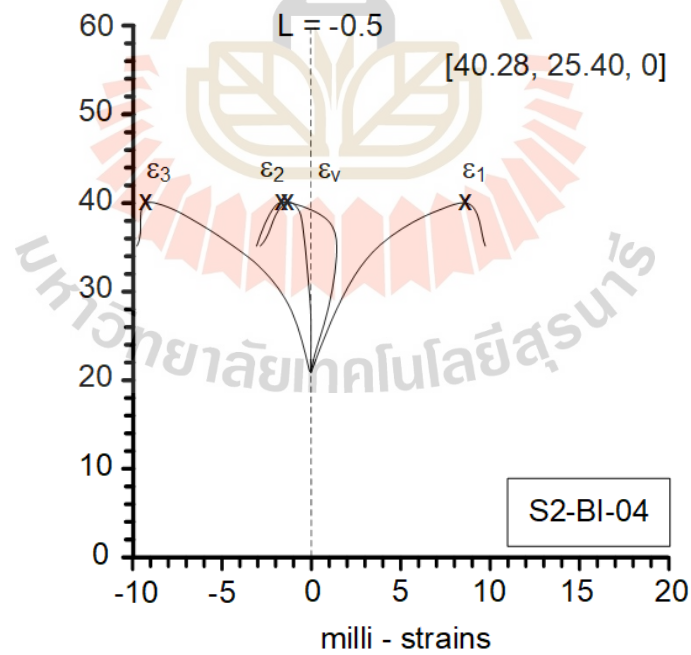
Figure A.24 Stress-strain curves of medium grained (Phu Phan) sandstone tested under σ_2 = 25.40 MPa and σ_3 = 0 MPa.
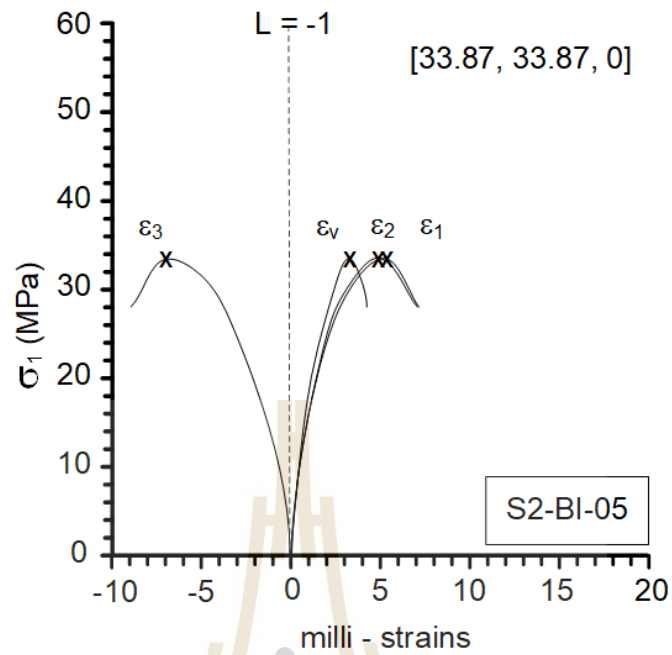
Figure A.25 Stress-strain curves of medium grained (Phu Phan) sandstone tested under σ_2 = 33.87 MPa and σ_3 = 0 MPa.
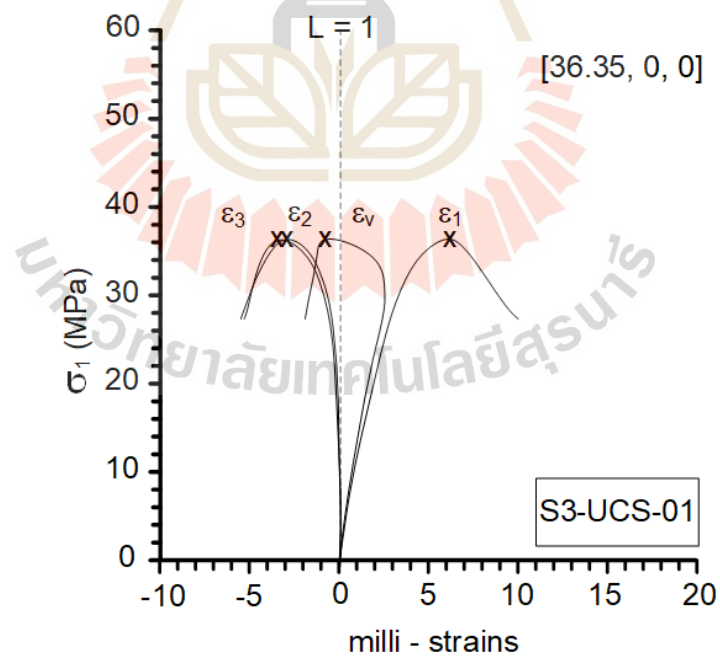
Figure A.26 Stress-strain curves of fine grained (Phu Phan) sandstone tested under σ_2 = 0 MPa and σ_3 = 0 MPa.
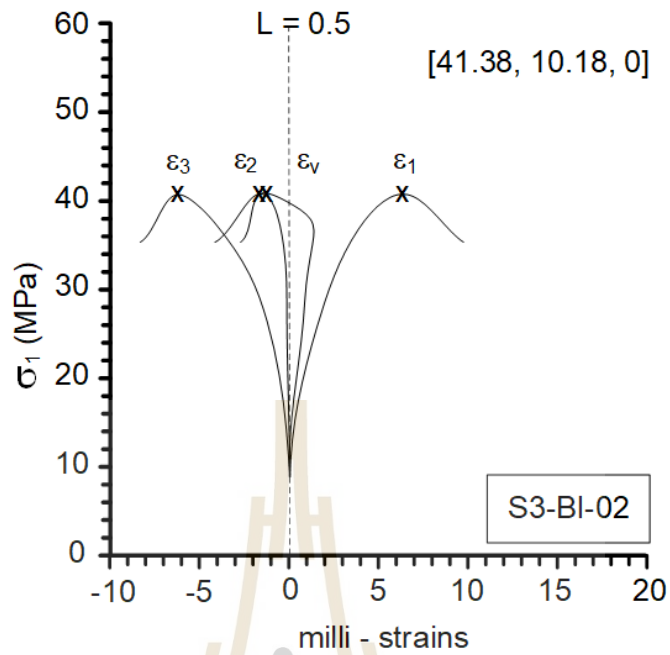
Figure A.27   Stress-strain curves of fine grained (Phu Phan) sandstone tested under
σ_2 = 10.18 MPa and σ_3 = 0 MPa.
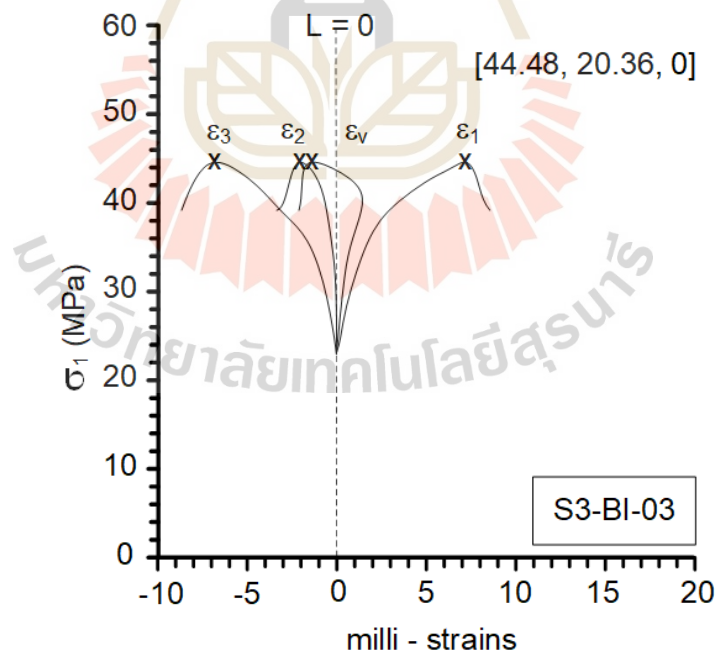
Figure A.28   Stress-strain curves of fine grained (Phu Phan) sandstone tested under
σ_2 = 20.36 MPa and σ_3 = 0 MPa.
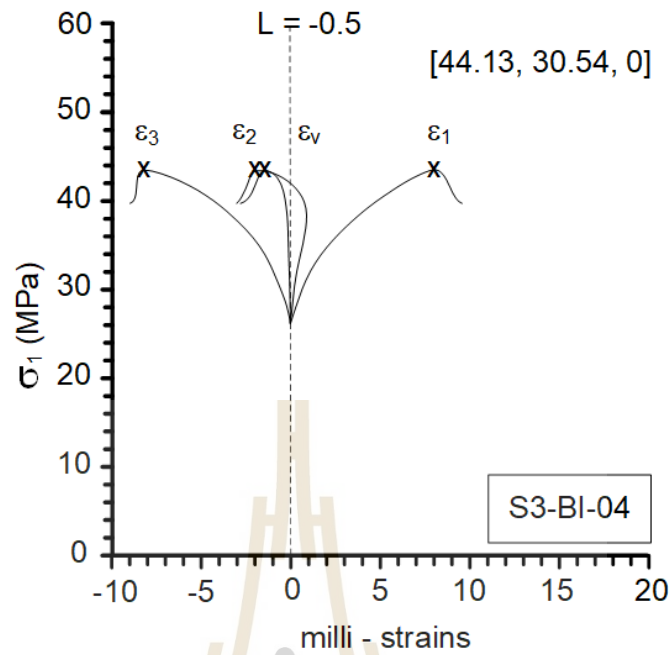
Figure A.29   Stress-strain curves of fine grained (Phu Phan) sandstone tested under
$\sigma_2 = 30.54$ MPa and $\sigma_3 = 0$ MPa.
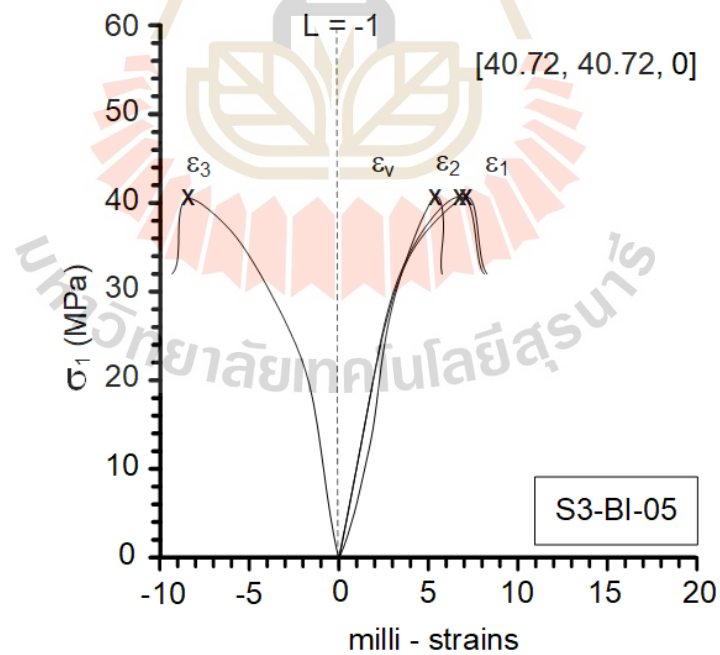
Figure A.30   Stress-strain curves of fine grained (Phu Phan) sandstone tested under
$\sigma_2 = 40.72$ MPa and $\sigma_3 = 0$ MPa.
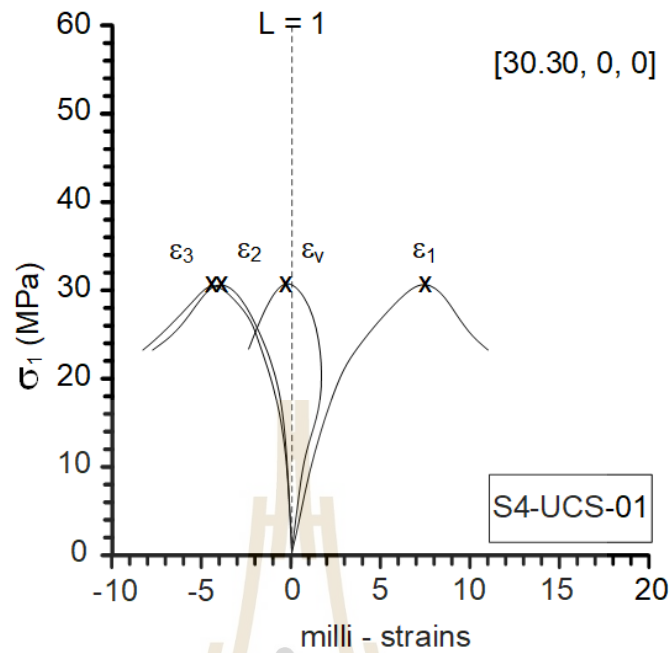
Figure A.31   Stress-strain curves of Fine grained (Phra Wihan) sandstone tested under σ_2 = 0 MPa and σ_3 = 0 MPa.
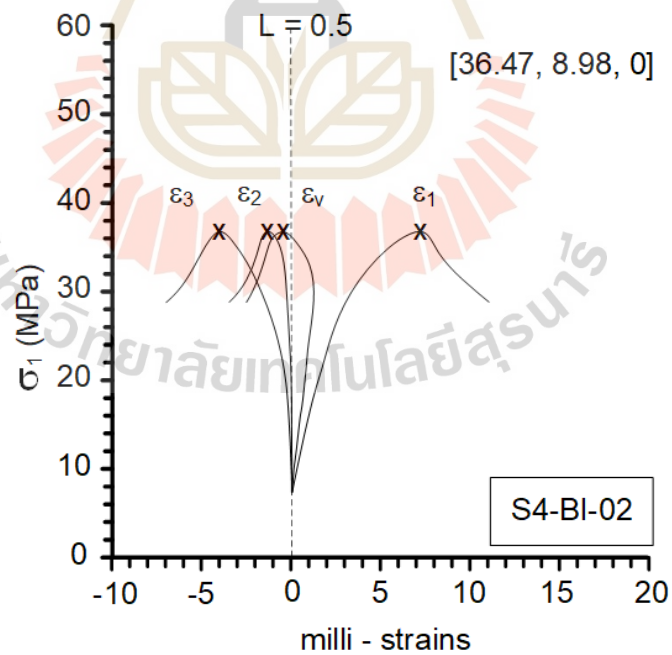
Figure A.32   Stress-strain curves of Fine grained (Phra Wihan) sandstone tested under σ_2 = 8.98 MPa and σ_3 = 0 MPa.
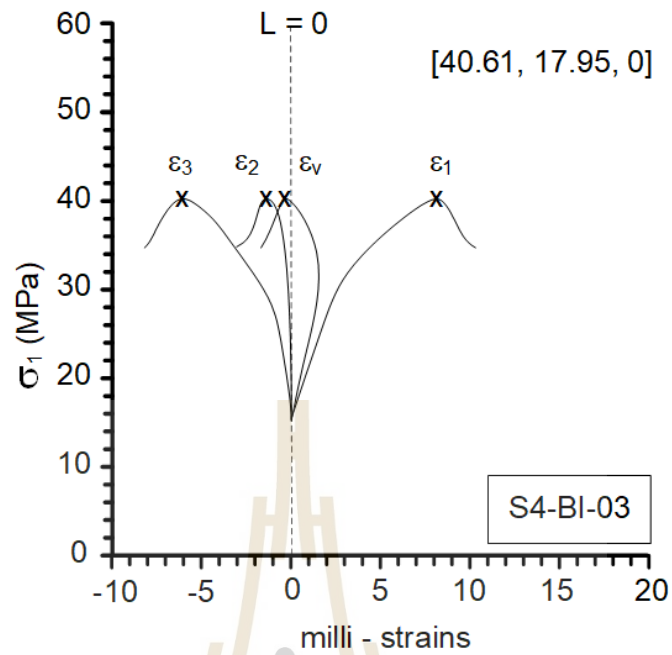
Figure A.33   Stress-strain curves of Fine grained (Phra Wihan) sandstone tested under
σ_2 = 17.95 MPa and σ_3 = 0 MPa.
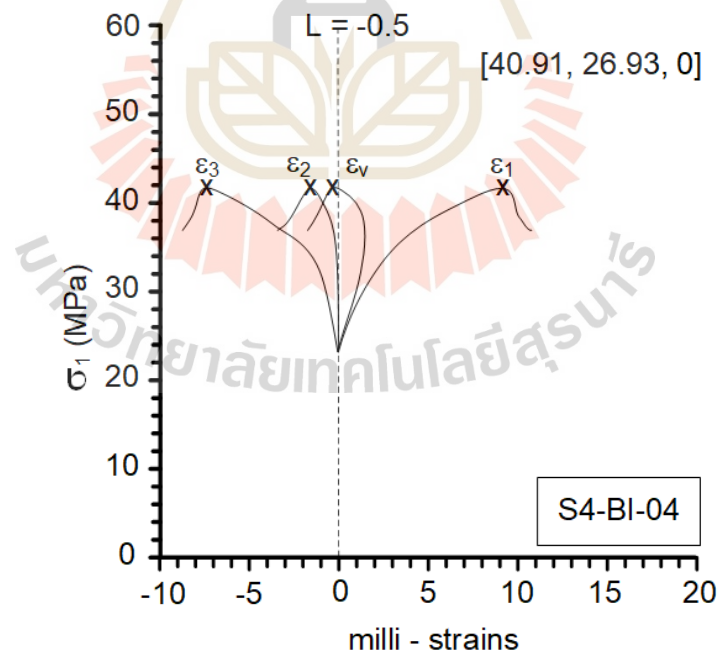
Figure A.34   Stress-strain curves of Fine grained (Phra Wihan) sandstone tested under
σ_2 = 26.93 MPa and σ_3 = 0 MPa.
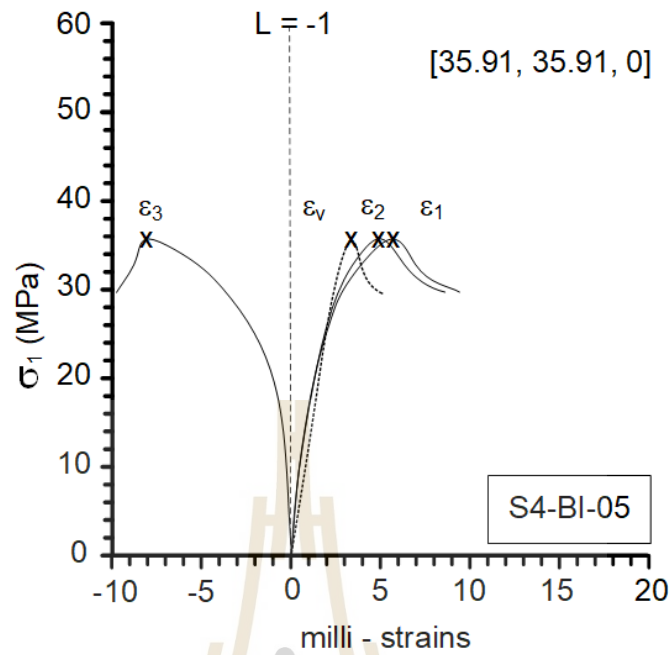
Figure A.35 Stress-strain curves of Fine grained (Phra Wihan) sandstone tested under
σ_2 = 35.91 MPa and σ_3 = 0 MPa.
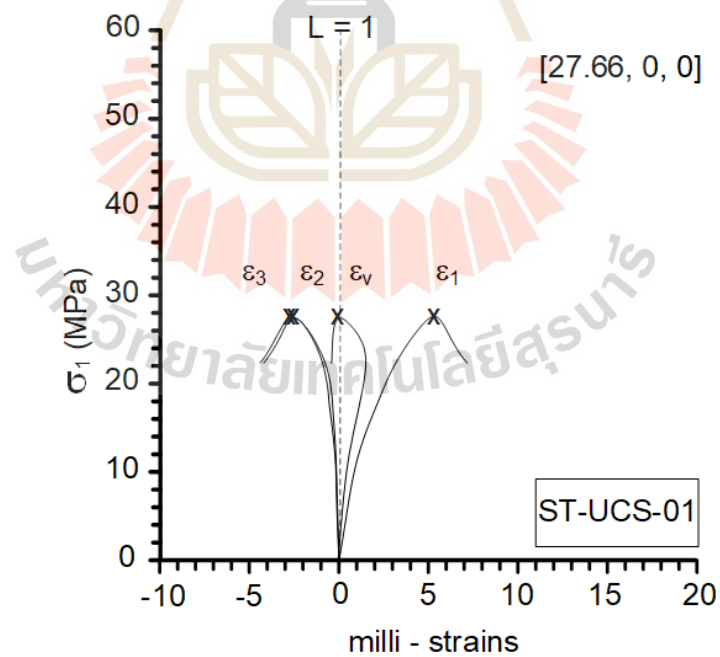
Figure A.36 Stress-strain curves of siltstone tested under
σ_2 = 0 MPa and σ_3 = 0 MPa.
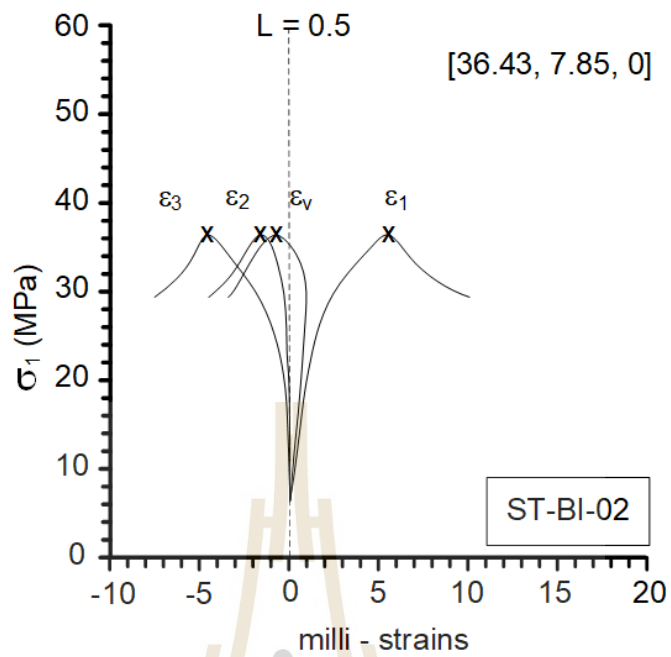
Figure A.37   Stress-strain curves of siltstone tested under
σ_2 = 7.85 MPa and σ_3 = 0 MPa.
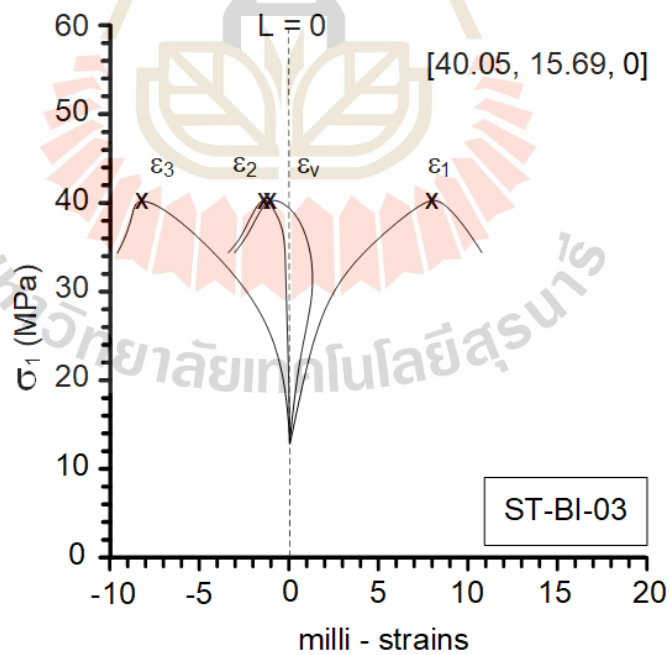
Figure A.38 Stress-strain curves of siltstone tested under
σ_2 = 15.69 MPa and σ_3 = 0 MPa.
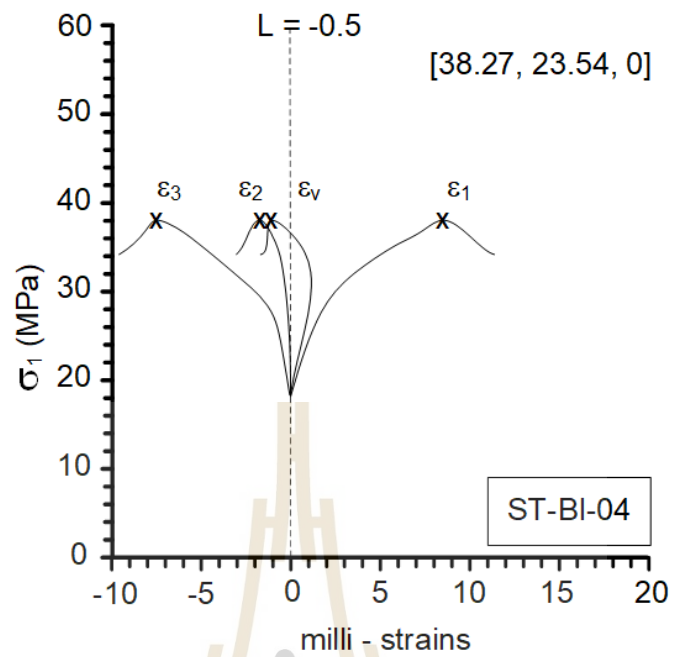
Figure A.39 Stress-strain curves of siltstone tested under
σ_2 = 23.54 MPa and σ_3 = 0 MPa.
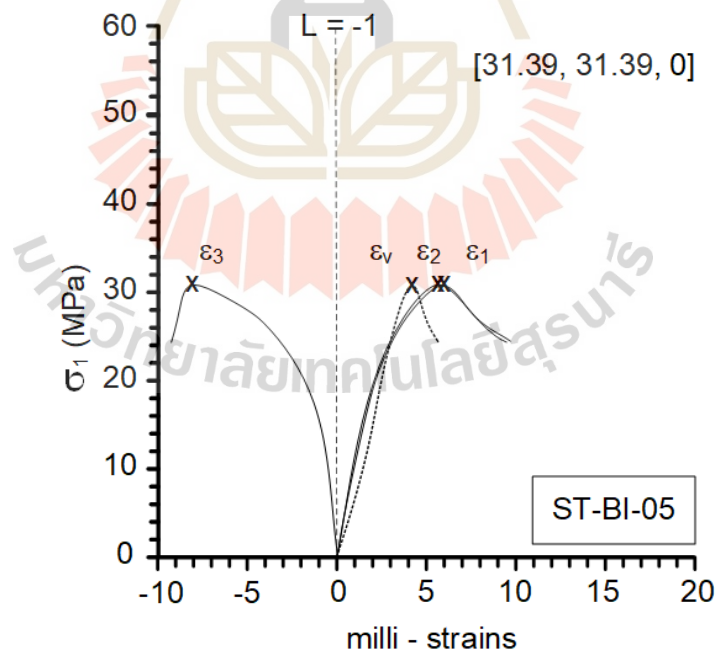
Figure A.40 Stress-strain curves of siltstone tested under
σ_2 = 31.39 MPa and σ_3 = 0 MPa.

BIOGRAPHY

Miss Nongnuchamas Panphuangkaew was born on January 2, 1998 in Phetchaburi Province, Thailand. She received her Bachelor's degree in Engineering (Geotechnology) from Suranaree University of Technology in 2020. For her post-graduate, she continued to study with a Master's degree in the Geological Engineering Program, Institute of Engineering, Suranaree university of Technology. During graduation, 2020-2023, she was a part time worker in position of research associate at the Geomechanics Research Unit and Georesources Research Unit, Institute of Engineering, Suranaree University of Technology. She has published one papers related to rock mechanics, titled Effect of Intermediate Principal Stress on Biaxial Compressive Strength of Rocks in the Proceeding of the Journal of King Mongkut's University of Technology North Bangkok. For her work, she is a good knowledge in geomechanics theory and practice.